CHALMERS
UNIVERSITY OF TECHNOLOGY

# Sub-synchronous controller interaction (SSCI) of series-compensated DFIG wind farms

## Analysis and damping of oscillations using STATCOM

Master's thesis in Electric Power Engineering

AHMED ELGAALI

Department of Energy and Environment
CHALMERS UNIVERSITY OF TECHNOLOGY
Gothenburg, Sweden 2016

# Sub-synchronous controller interaction (SSCI) of series-compensated DFIG wind farms

Analysis and damping of oscillations using STATCOM

AHMED ELGAALI


CHALMERS
UNIVERSITY OF TECHNOLOGY

Department of Energy and Environment
*Division of Electric Power Engineering*
Chalmers University of Technology
Gothenburg, Sweden 2016

Sub-synchronous controller interaction (SSCI) of series-compensated DFIG wind farms
Analysis and damping of oscillations using STATCOM
AHMED ELGAALI



Supervisor: Dr. Richard Rivas, ABB FACTS
Examiner: Prof. Massimo Bongiorno, Energy and Environment

Department of Energy and Environment
Division of Electric Power Engineering
Chalmers University of Technology
SE-412 96 Gothenburg
Telephone +46 (0)31-772 1152

# Abstract

One of the problems faced by the integration of large renewable energy sources -such as wind turbines- is that often the load centres are very far from the production centres. This forces the use of series capacitor compensation in order to increase the power transfer and the transient stability limits. The presence of series compensation introduces resonance into the system and this resonance could interact with the control system of the connected DFIG wind farm, thus causing the system (under certain conditions) to experience unstable resonant oscillations at the sub-synchronous frequency range.

This thesis studies the sub-synchronous controller interaction (SSCI) of DFIG-based wind-farms with series-compensated transmission lines and suggests a STATCOM solution to damp the resulting oscillations. This is done by studying the IEEE First Benchmark Model (FBM) for computer simulation of sub-synchronous resonance as test system. Analysis is conducted in both time domain and frequency domain to understand the parameters that affect the system's stability and create the unstable sub-synchronous oscillations. The software employed is PSCAD/EMTDC. The frequency-domain analysis includes the use of the net positive damping criteria to assess the stability of the system

For the mitigation of the SSCI oscillations, a STATCOM installed at the DFIG wind farm bus is employed. It is assumed that this STATCOM is there for the purpose of reactive power compensation and grid code compliance of the wind farm. For SSCI oscillation damping, a controller is designed and tested. The damping controller is based on detecting the presence of sub-synchronous oscillation and then determining its frequency on-line. Next this frequency is used to extract the unstable component from the active power signal. This extracted signal is then multiplied by an empirical gain and afterwards used to modulate the voltage reference of the STATCOM voltage controller. This method was found to damp both oscillations on voltage and power signals.

# Acknowledgement

This work was conducted at ABB FACTS. I would like to thank them for opening this opportunity.

My thanks go to my supervisor Richard Rivas for his valuable support during all the project steps. I would also like to thank Professor Massimo Bongiorno, my examiner for his support and direction through the thesis and his thorough discussions. My thanks extend to Hector Latorre for his continuous support in PSCAD and other issues. I thank Tomas Baeza, Shane Hutchinson, Peter Olofsson, Mohsen Assodar, Magnus Tarle, Hemant Kumar, Marcio De Oliveira, Yigen Zenlander.

Thanks and gratitude are extended to the Swedish Institute SI (Svenska Institutet) for granting me the study scholarship to come and study in Sweden.

Finally, I would like to thank my family for their continuous support despite their distance and all my friends specially the ones here in Sweden (Alaadin, Mazin, Amal and Saher)

Ahmed Elgaali
August 2016
Västerås, Sweden

# Contents

# List of Figures

# List of Tables

# 1

# Introduction

## 1.1 Background and thesis motivation

Worldwide the installed wind power capacity has grown by almost the double between 2011 and 2015 [10]. However, wind energy is often delivered from locations far away from the load centres. This long distance makes the use of series capacitors inevitable to compensate for the inductance of the AC transmission lines. Thus the system's transient stability improves and the transmission line's capacity increases which is beneficial both on a technical level and on an economical level as well. [20].

One of the issues related to the presence of series capacitors in the transmission lines is the possibility of introducing series resonances below the grid's fundamental frequency. These resonances could interact in an unstable manner with the torsional modes of neighbouring generator-turbine sets. This phenomenon is called sub-synchronous resonance (SSR) and is well known now -since it first appeared 45 years ago [14]. A lot of research has been produced around this topic and the industry has now good experience in dealing with it and mitigating it.

A new sub-synchronous issue is due to the interaction between the power electronics controller of some components (such as the converters in the DFIG wind generator or the HVDC) and the series-compensated network. It is referred to with the term Sub-Synchronous Controller Interaction (SSCI) which, in a broader term, is the interaction between the series-compensated line and any neighbouring power electronics device controller. This phenomenon is purely electric since the turbine's mechanical system is not involved in the event. If the turbine's system interacts with a neighbouring power electronics controller, then this type of interaction is termed as Sub-Synchronous Torsional Interaction (SSTI) [2].

The DFIG-based wind-farms were thought to be immune to sub-synchronous events, but in 2009 an event occurred in a 200-MW wind-farm in Texas, which resulted in growth of voltage to a peak of 2 pu and the activation of crowbar in a number of generators.

The purpose of this thesis work is to study in the first part the DFIG wind-farm sub-synchronous characteristics and its susceptibility to SSCI. In the second part, a solution will be implemented to damp the SSCI using a STATCOM connected to the DFIG wind-farm bus.

## 1.2 Objectives

The main objectives of this thesis are to evaluate the risk of SSCI in DFIG wind-farm installations and to damp these oscillations using STATCOM's.
The following steps will be carried out to reach the objectives:

1. Obtain harmonic frequency scan of the DFIG wind-farm in the sub-synchronous frequency range looking at the wind-farm from its output. This is done by injecting harmonic voltage and measuring the current and then applying FFT to the measured current

2. Evaluate the stability of the system comprised by DFIG wind-farm connected to a series compensated network using the net-positive damping criterion. This is done by using Nyquist stability criterion on the open loop system of the DFIG wind farm and the network. This requires the use of the previously obtained harmonic impedance scan.

3. Design a controller for the STATCOM to provide SSCI oscillation damping.

## 1.3 Thesis Structure

Chapter 1 introduces to the SSCI by giving a background to the problem. Also it describe the thesis objectives and its outline.

Chapter 2 gives an introduction to the definitions related to sub-synchronous oscillations in power systems and the application of FACTS devices to damp and mitigate them.

Chapter 3 introduces the reader to the concept of the DFIG and some details on its circuit representation and control strategy.

Chapter 4 explains the proposed methodology for the analysis of the SSCI as well as the model used for the study. Also the proposed STATCOM control strategy is presented.

Chapter 5 presents the results of the proposed methodology for oscillations.

Chapter 6: Gives conclusions about the most important findings in the thesis and the proposed future work.

# 2

# Theory

## 2.1 Introduction

This chapter introduces the different elements that contribute to the SSCI, which are the series-compensated transmission line and DFIG-based wind turbines. For the series compensation, both its purposes and the basic theory behind it are introduced. As for the wind turbine, there is a short introduction to the different types of wind turbines, but the focus is on the Doubly-Fed Induction Generator (DFIG), which is also referred to as Type-3.

## 2.2 Wind Turbine Systems

### 2.2.1 Fixed-Speed Wind Turbine (Type-1)

It consists of a gear-box that couples the wind-turbine to a squirrel-cage induction generator, which is directly connected to the grid by a step-up transformer, as shown in Fig. 2.1. Speed is fixed and power is generated when the turbine's speed is faster than the electrical frequency, which creates negative slip.

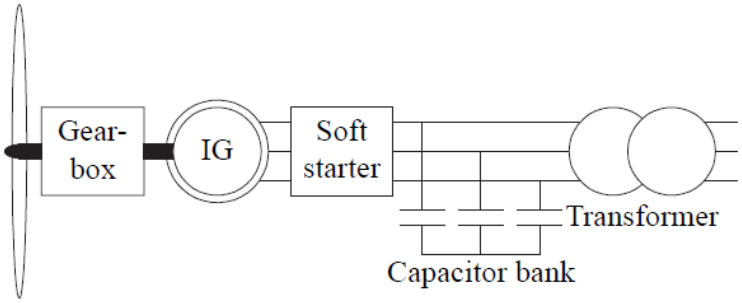


**Figure 2.1:** Fixed-Speed wind turbine (Type-1) [26]

### 2.2.2 Limited-variable speed (Type-2)

In this type a there is a wound-rotor induction generator that is connected directly to the grid through a step-up transformer just, as in Type-1. In addition to that, a variable resistor is connected to the rotor circuit. A set of resistors and power electronics are used to implement the variable resistor external to the rotor via slip rings. This configuration controls the rotor currents, which keep the power constant at the wind power plant terminal even during wind speed changes.

### 2.2.3 Doubly-Fed Induction Generator (Type-3)

It is the next level of Type-2 wind generators and it is obtained by adding a full variable frequency converter instead of the rotor resistors as shown in Fig. 2.3. The next section will explain its operation principle in details.

### 2.2.4 Full-Converter wind turbine (Type-4)

It consists of generator (squirrel-cage induction generator or synchronous generator) which is connected to a back-to-back converter which in turn is coupled to the grid through a transformer. The main advantage of this type of turbines is the robust and well developed control [26]. The main disadvantage is that the converter is rated to the full power of the generator, which means a more expensive system.

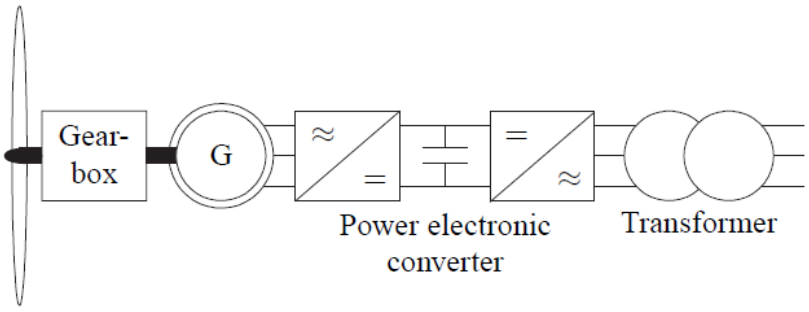


**Figure 2.2:** Full-converter wind turbine (Type-4) [26]

## 2.3 Doubly-Fed Induction Generator (DFIG)

### 2.3.1 Principle of DFIG Operation

DFIG is a wound-rotor induction generator with its rotor fed through a back-to-back converter. The rotor is excited by a variable frequency voltage source converter

(VSC) which adjusts the rotor current by slip rings. This converter controls the output active and reactive power from the generator by controlling the rotor current both in magnitude and phase. The general setup is shown in Fig. 2.3.

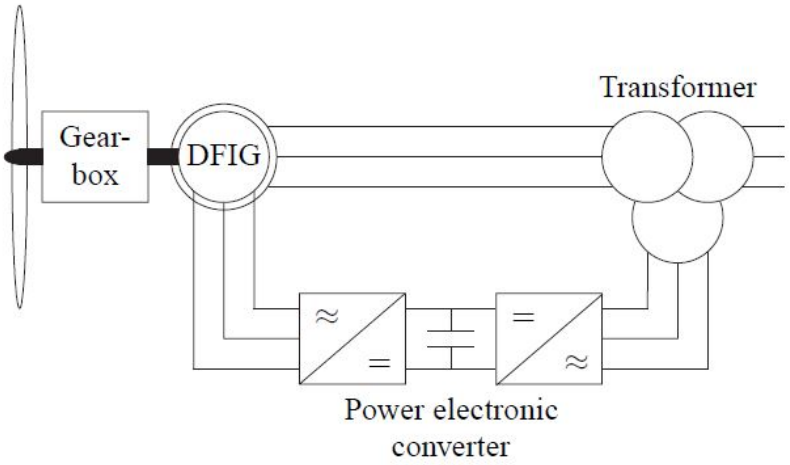


**Figure 2.3:** Variable-speed wind turbine with Doubly-Fed Induction Generator [26]

Fig. 2.3 depicts the wound-rotor generator with its stator connected to the grid and a back-to-back VSC (rotor-side and grid-side) with a dc link. Rotor's windings are connected to the Rotor-Side Converter (RSC) via slip rings. This RSC is supplied by another VSC that is connected to the grid, hence named Grid-Side Converter (GSC). At the DC link between the two converters a capacitor is placed to minimise the voltage ripple during switching of the converters. Moreover, a grid filter is connected to the GSC to reduce the harmonics from the converter ($R_f$ and $L_f$ in Fig. 2.4).
As a result of this configuration the generator can operate on different wind speeds. One thing to be noted is that the size of this back-to-back converter is typically in the range of 15%-30% of the rated power of the wind turbine. This is due to the fact that it handles only the slip power, which is an important advantage of the DFIG.

### 2.3.2 Doubly-Fed Induction Generator Equivalent Circuit

The DFIG is essentially a wound rotor induction generator which is represented by the cage-bar induction generator circuit with the difference that the rotor-side circuit is fed by another source. The Γ model is used to represent the machine because of its simplicity in obtaining the controller. Fig. 2.4 illustrates this model:

Where:
$\underline{v}_S$ : stator voltage;
$\underline{v}_R$: stator voltage;
$\underline{i}_S$: stator current;

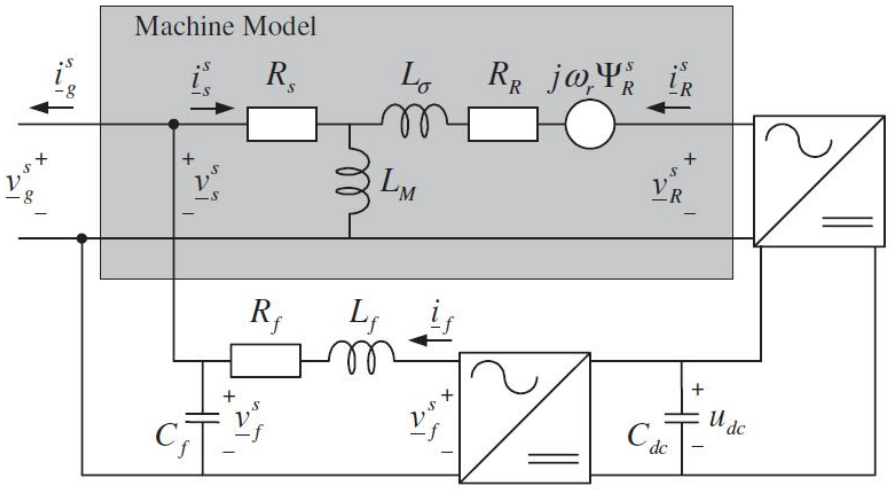


**Figure 2.4:** Doubly-Fed Induction Generator Equivalent Circuit [21]

$\underline{i}_R$: rotor current;
$\underline{R}_S$: stator resistance;
$\underline{R}_R$: rotor resistance;
$\underline{\Psi}_S$: stator flux vector;
$\underline{\Psi}_R$: rotor flux vector;
While the flux linkage in the stator and rotor is expressed as [21]:

$$\underline{\Psi_S^S} = L_M(\underline{i_S^S} + \underline{i_S^S}) \tag{2.1}$$

$$\underline{\Psi_R^S} = (L_\sigma + L_M)\underline{i_R^S} \tag{2.2}$$

$$T_e = 3n_p I_m\{\underline{\Psi_S^S} Conj(\underline{i_R^S})\} \tag{2.3}$$

Where:
$L_M$: Magnetising inductance.
$L_\sigma$: Leakage inductance.
$n_p$: number of pairs of poles.
In addition, Fig. 2.5 shows the DFIG equivalent circuit representation in steady-state using the $j\omega$ notation.

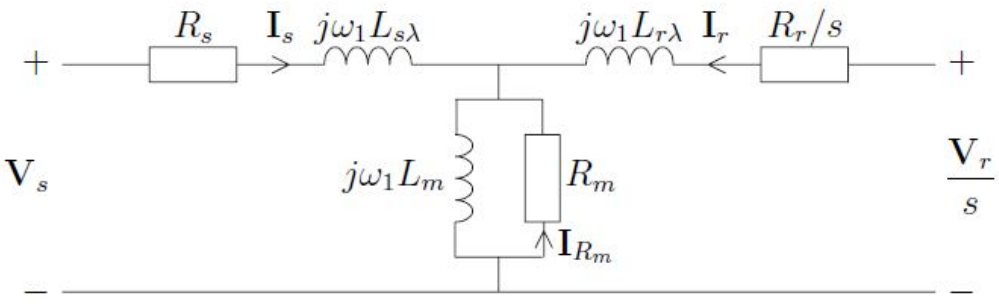


**Figure 2.5:** DFIG Equivalent Circuit in Steady-State [26]

### 2.3.3 DFIG control [21]

The DFIG control consists of two main controllers: one is for the Rotor-Side Converter (RSC) and the other is the Grid-Side Converter (GSC). The RSC controller is responsible for DFIG terminal active and reactive power while the GSC controller takes care of the voltage of the DC-link between the RSC and GSC.
The control system is a vector control system based on a rotating coordinates system which has two components: $q$- and $d$-components. The stator voltage vector is aligned with the $q$-component creating the so called flux-oriented coordinates system. This method of control makes it easier to control AC quantities in steady-state, where the voltage and current vectors are "seen" as dc quantities with respect to the new coordinate system.

#### *RSC Controller*

The control of the RSC has a cascaded control structure, which means that there are two control loops: inner and outer. The inner loop is a current control loop (CC), which is the faster one and it creates the voltage reference for the rotor from the given active and reactive power. The outer loop is the slower one. It consists of two controllers: active and reactive power controllers. Those two loops create the $d$ and $q$ current references for the current controller. The inputs to the outer loop are both measured and compared with the reference values for both active and reactive power.
The controller is in rotating coordinates aligned to the DFIG stator flux.

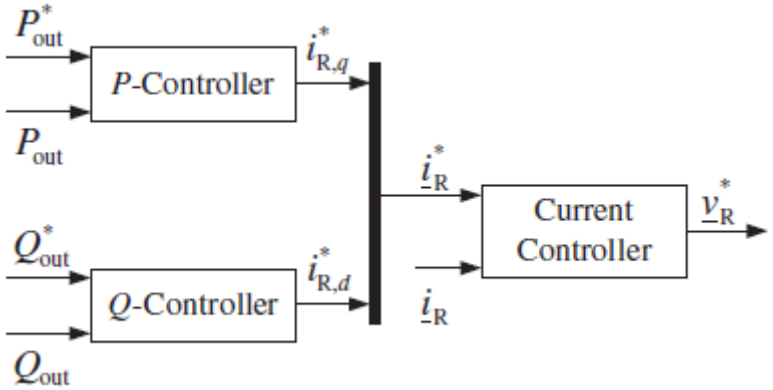


**Figure 2.6:** General control scheme for RSC: showing the inner (current) and outer (power) control loops [21]

***Active and reactive power controller***: It consists of two PI controllers for both real and reactive power. These two controllers produce two reference currents. The real power controller produces the $q$-component of the rotor current ($i^*_{R,q}$) while the reactive power controller produces the $d$-component ($i^*_{R,d}$). The controllers equa-

tions are as follows:

$$\begin{aligned} i^*_{R,q} &= K_{p,P}\left(1+\frac{1}{sT_{i,P}}\right)(P^*_{out}-P_{out}) \\ i^*_{R,d} &= K_{p,Q}\left(1+\frac{1}{sT_{i,Q}}\right)(Q^*_{out}-Q_{out}) \end{aligned} \tag{2.4}$$

where for the PI controller, the $K_p$ is the proportional gain and the $T_i$ is the integrator time constant.

***Damping term***: This term is added to give more damping to the drive system. This term is implemented by passing the rotor speed through a high-pass filter, which has a time constant that depends on the frequency of oscillations to be damped. This removes the oscillatory component of the rotor speed.

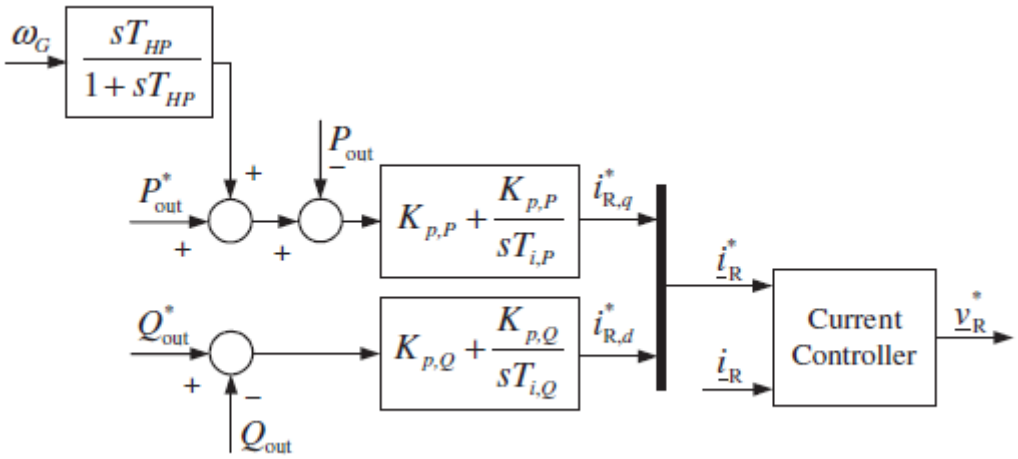


**Figure 2.7:** Detailed control scheme for RSC: showing details of the outer control loop plus the damping term [21]

***RSC Current controller***:It has the following control law:

$$\underline{v}^*_R = \frac{1}{sT_{LP}+1}\hat{e}_{emf} + j\omega_2 L_\sigma \underline{i}_R + K_{p,cc}(\underline{i}^*_R - \underline{i}_R) \tag{2.5}$$

where, for the proportional controller, $K_{p,cc}$ is the proportional gain. The term $\underline{\hat{e}}_{emf}$ is the estimation of the machine's back emf. This estimation goes through a low-pass filter with time constant $T_{LP}$. The reason that there is no integral part for the current controller (only proportional part) is that the outer loop (power controllers) already contains an integral term which removes the need for it in the inner loop. The current controller gain is expressed as follows

$$K_{p,cc} = \alpha_{cc} L_\sigma \tag{2.6}$$

Where $\alpha_{cc}$ is the current controller bandwidth and $L_\sigma$ is the leakage inductance.

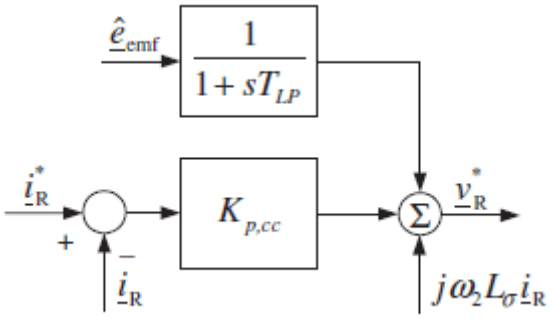


**Figure 2.8:** RSC current controller [21]

### *GSC Controller*

Fig. 2.3.3 shows the general GSC control scheme. As the RSC controller, it has two loops: the inner is again a current controller that takes the current reference from the outer loop and gives out the voltage reference of the filter ($\underline{v}_f^*$), while the outer loop is the DC link voltage controller. The details for this controller are as follows:

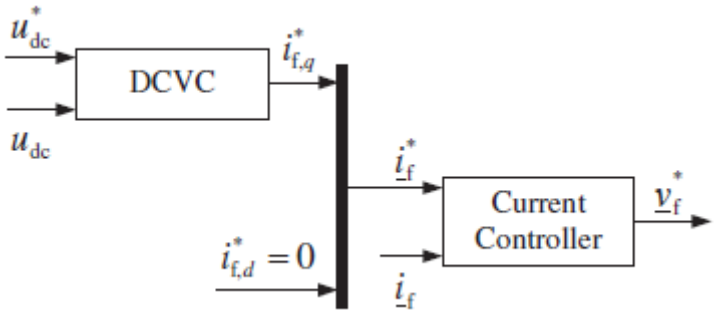


**Figure 2.9:** RSC current controller [21]

***DCVC (DC-link Voltage Controller)***: This is the outer loop that produces the $q$-component of the grid filter current $i_{f,q}^*$. Here, the control of the DC-link voltage is considered to be the control of the flow of active power through the voltage-source converter, which is assumed to be ideal. Also, assuming that the capacitance of $C_{dc}$ in Fig. 2.4 is constant, it can be concluded that the power flow through the DC-link ($P_{dc}$) equals the capacitor's energy $_{dc}$ as follows:

$$P_{dc}(t) = \frac{dw_c}{dt} = \frac{1}{2} C_{dc} \frac{du_{dc}^2(t)}{dt} \tag{2.7}$$

Since the power through the dc capacitor is a function of the rotor power ($P_R$) and also of the power output of the grid-side converter ($P_f$), then linearizing Eqn: 2.7 gives the following:

$$\frac{1}{2} C_{dc} u_{dc.0} \frac{d\Delta u_{dc}}{dt} = P_{dc} = -\Delta P_R - \Delta P_f \tag{2.8}$$

The control law for the DCVC is as follows:

$$i_{f,q}*(s) = \left(K_{p,dc} + \frac{K_{i,dc}}{s}\right)[u_{dc}^{*2} - u_{dc}^2] - P_R \tag{2.9}$$

Where $K_{p,dc} = \alpha_{dc} C$. Typical values for the $\alpha_{dc}$ are about one tenth of the current controller's bandwidth $\alpha_{cc}$.

***RSC current controller***: As in the RSC current controller, the following control law is derived:

$$\underline{v}_f = \frac{1}{sT_{LP} + 1} \hat{v}_c + j\omega_s L_f \underline{i}_f + K_{p,cc}(\underline{i}_f^* - \underline{i}_f) \tag{2.10}$$

Where the proportional gain is

$$K_{p,cc} = a_{cc} L_f \tag{2.11}$$

.

***Phase-Locked Loop (PLL)***

As was stated earlier, the control system is derived in a rotating coordinate system that is aligned to the grid voltage vector and rotates with its frequency counterclockwise. In order to align the coordinate system to the voltage grid voltage vector, it is essential to know the voltage angle at all times. This is done by a Phase-Locked Loop (PLL) which has the following law:

$$\begin{aligned} \dot{\hat{\omega}}_s &= \alpha_{PLL}^2 \varepsilon_{PLL} \\ \dot{\hat{\theta}}_s &= \hat{\omega}_s + 2\alpha_{PLL} \varepsilon_{PLL} \end{aligned} \tag{2.12}$$

Where $\hat{\theta}_s$ is the estimate of the grid voltage angle while $\hat{\omega}_s$ is the estimated grid angular frequency and $\varepsilon_{PLL}$ is the PLL input error. Fig. 2.10 illustrates the PLL block diagram.

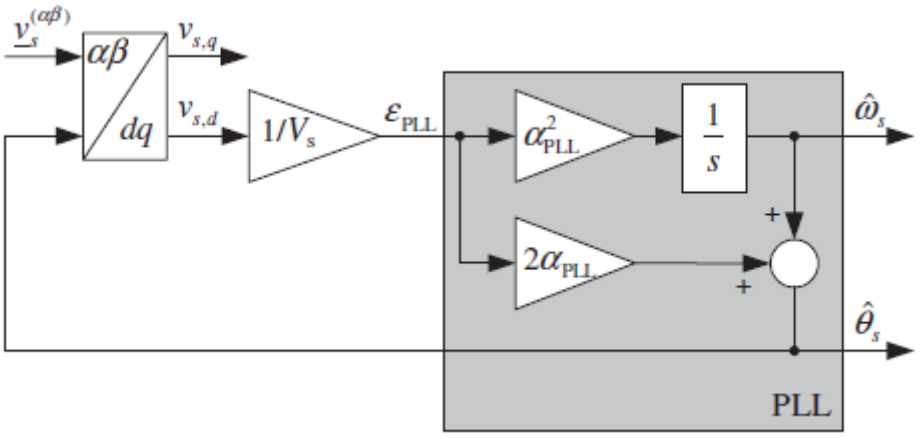


**Figure 2.10:** PLL for estimating grid voltage angle [21]

## 2.4 Series Compensation

### 2.4.1 Introduction

It is a well-established fact that the length of the AC transmission lines limit their power-carrying capabilities. The longer the line is, the larger its series reactance

becomes, which is inversely proportional to the transmitted power. In order to minimise the line reactance, fixed capacitive series compensation has been used to introduce negative series reactance and hence reducing the effective line impedance. The series compensation can also be variable

The introduction of controlled series capacitive compensation such as TCSC (Thyristor-Controlled Series Capacitor) was proven to improve transient stability and to render the line power flow controllable, in addition to increase the transmission line's capacity to a very high degree. Controllable series line compensation is a cornerstone of FACTS technology. It can be applied to achieve full utilization of transmission assets by controlling the power flow in the lines, preventing loop flows, and with the use of fast controls, minimizing the effect of system disturbances, thereby reducing traditional stability margin requirements [17].

### 2.4.2 Principle of Series Compensation

As was mentioned before, the idea is to increase the power transmitted over a line by decreasing the overall line impedance according to

$$P = \frac{V^2 sin\delta}{X} \tag{2.13}$$

where, referring to Fig. 2.11 V is the magnitude of $V_s$ and $V_r$ at the sending and receiving ends, respectively and X is the line impedance.
The effective transmission line impedance including the series compensation $X_{eff}$ is expressed as:

$$X_{eff} = X - X_C = (1 - k)X \tag{2.14}$$

where $X_C$ is the capacitive reactance of the series capacitor and $k = \frac{X_C}{X}$ is the compensation level.

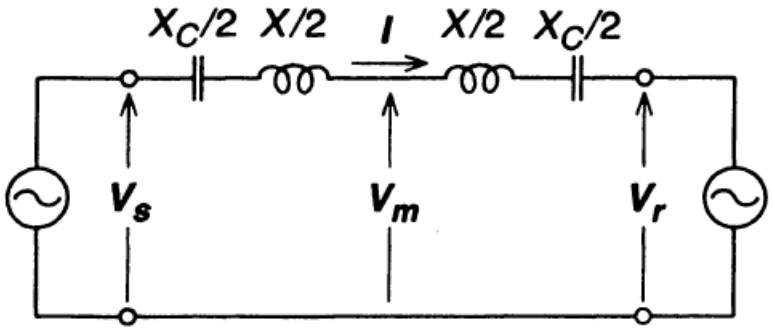


**Figure 2.11:** Simple Two-machines and transmission line network [17]

The current and active power flowing in the compensated line can be written as:

$$I = \frac{2V}{(1 - k)X} sin\frac{\delta}{2} \tag{2.15}$$

$$P = V_m I = \frac{V^2}{(1-k)X} sin\delta \tag{2.16}$$

While the reactive power delivered by the series capacitor is:

$$Q_C = I^2 X_C = \frac{2V^2}{X} \frac{k}{(1-k)^2} (1 - cos\delta) \tag{2.17}$$

The interpretation of the series compensation concept is that according to Eqn.2.13 in order to increase the power flow of a line, the line impedance should be decreased. The series capacitor cancels portion of the line reactance according to Eqn. 2.14 rendering it smaller in effect. Another interpretation is that in order to increase the power flow, it is essential to increase the current flowing in the line which means that the voltage across this line needs to be increased, hence a series voltage source is needed for the line. The series capacitor does this job by introducing an opposite voltage to the original voltage.
The concept of fixed series capacitor has been extended to a variable series compensation. This can be obtained by variable reactive impedance or by a series voltage source [17]. There are different approaches to obtain variable impedance series compensation such as: GTO Thyristor-Controlled Series Capacitor, Thyristor-Switched Series Capacitor (TSSC), and Thyristor-Controlled Series Capacitor (TCSC).

### 2.4.3 Applications of Series Compensation

In addition to the main purpose of the series compensation which is the increase of active power flow in transmission lines, other important applications exist. They are:

- Voltage Stability: Minimise voltage variations at the receiving end by reducing series reactive impedance.

- Transient Stability Improvement: Reducing the effective line impedance increases the transmitted power over the line hence improving the transient stability. And one of the main areas of this application is the wind generation since the wind turbines are usually situated at remote places away from the load centres; long transmission lines are hence needed.

- Power Oscillation Damping: Using controlled series compensation to damp low-frequency power oscillations in the line

- Sub-synchronous Oscillation Damping: Controller series compensation is used to directly affects the line impedance at the sub-synchronous frequencies.

### 2.4.4 Summary

This chapter discussed the main components contributing to the problem of SSCI. Different types of wind-farms were briefly described. Then, the operating principle of the DFIG wind-farm isintroduced with details of the circuit and more details on the DFIG control system. Finally, a section on series-compensation introduced its basic concept and applications.

# 3

# Sub-Synchronous Resonance in Power Systems

## 3.1 Introduction

This chapter introduces the reader to the general problem of sub-synchronous resonance in power systems by listing the different types of SSR and the reason of their occurrence, in addition to which components of the power system contribute to each type. Then in the second section, the problem of SSCI in DFIG wind farms is treated by giving more details on the components of the DFIG drive to which the instability is attributed, and hence the SSR. Next, the third section introduces the methods of analysis used to investigate the SSR in DFIG wind farms. Finally in the fourth section, the results of the analysis are shown and discussed.

## 3.2 Definitions and classifications of SSR

The IEEE defines the SSR as follows [32] :
***Subsynchronous resonance is an electric power system condition where the electric network exchanges energy with a turbine generator at one or more of the natural frequencies of the combined system below the synchronous frequency of the system.***

It is clearly seen from the definition that the SSR is between the power system and a generator-turbine set. However, a more generic definition of the SSR includes different causes of the SSR other than the mechanical system of the generator-turbine set and hence named sub-synchronous interaction as will be discussed below.

- Sub-Synchronous frequency

It is the frequency of oscillation that is below the power system's rated frequency (50 or 60 Hz)

- SSI: Sub-Synchronous Interaction

  This is a generic term that refers to the interaction of one of the elements of the power system when they exchange energy at one or more of the system's sub-synchronous modes (natural frequencies) of the combined system.

- SSO: Sub-Synchronous Oscillations

  A generic term that refers to the oscillation that result from the SSI mentioned before.

- SSR: Sub-Synchronous Resonance

  It is a more particular definition that refers to the interaction of the generator-turbine set of a synchronous generator with the effective impedance of an electrically close series compensated network.
  The frequency of electrical resonance is given as:

$$f_{er} = \pm f_s \sqrt{\frac{x_c}{x_L}} \tag{3.1}$$

  where $f_s$ is the network's synchronous frequency, $x_c$ is the series capacitor's reactance and $x_L$ is the network's total reactance. Now, since this is the resonant frequency, then any small disturbance in the network will excite currents at at the stator at $\pm f_{er}$. The positive-sequence component of this stator current induces stator flux at this frequency, which in turn produces rotor currents at frequency $f_r = f_0 - f_{er}$, where $f_r$ is the electrical frequency of the rotor.

- IGE: Induction Generator Effect

  This is a purely electrical phenomenon where the series compensated network resonates with the synchronous machine (and not the generator-turbine set), which implies the assumption that the mechanical system is rigid. The synchronous generator, seen from the standpoint of the stator flux that rotates at sub-synchronous frequency, behaves as an induction generator. In this phenomenon, the resistance of the rotor windings seen from the point of view of the stator at the sub-synchronous frequencies is negative. This can be shown as follows: the slip at sub-synchronous frequency is [2]:

$$S_{ssr} = \frac{f_{er} - f_0}{f_{er}} \tag{3.2}$$

And, referring to the DFIG equivalent circuit in Fig. 2.5, the rotor resistance at the sub-synchronous frequency is [2]:

$$R_{eq}^{ssr} = \frac{R_r}{S_{ssr}} \tag{3.3}$$

The rotating flux resulting from the armature currents at the sub-synchronous frequency rotates in a frequency $f_{er}$ which is slower than the rotor electrical frequency $f_0$ which, according to Eqn. 3.3, results in a negative slip of the induction machine, which in turn gives a negative resistance of the rotor according to Eqn. 3.2 [30]. If the sum of this resistance $R_{eq}^{ssr}$ and the armature and network resistances at the network's resonant frequency is less than zero; then self-excitation could occur and hence sub-synchronous currents will grow [30].

- SSCI: Sub-Synchronous Controller Interaction

This interaction, which is the main focus of this thesis, is the oscillation between a series compensated line and a power electronics controller (such as HVDC, PSS or DFIG controllers), which has fast response to speed or power in the sub-synchronous range. It falls in the category of device-dependent sub-synchronous oscillations according to the IEEE Guide of SSR [31].
Due to this nature, then SSCI does not include any mechanical interaction (as opposed to SSR and SSTI). The cause of these oscillations is the fact that the DFIG system exhibits negative resistance in the sub-synchronous oscillations range (negative damping), which causes the oscillations in this frequency range to grow.
Since this is the type of oscillation treated in this thesis, more details will be presented in the next chapter.

## 3.3 SSR Analysis Methods

Whatever the type of SSR is, an important step towards evaluating it is its analysis. After obtaining an accurate model of the system, different methods of analysis could be applied to the system. These methods are either in time domain or in frequency domain. For time domain simulations, electromagnetic transient software such as PSCAD/EMTDC can be used.
The purpose for SSR analysis is to detect the presence of SSR conditions under different systems contingencies to, evaluate the severity of these conditions, and to study the effect of different control and operation conditions on the sub-synchronous oscillations [25].

### 3.3.1 Time-Domain simulations

For this approach, a detailed model of the system to be studied is developed in an electromagnetic transient software such as PSCAD/EMTDC. Such a software represents both electromagnetic and electromechanical systems by their differential equations and calculates the solution to these equations for a certain fixed time step [11].
The results of this analysis are time domain plots that show the presence of oscillations in electrical quantities (power, voltage and current...) and/or mechanical quantities (speed, torque...) that oscillates in sub-synchronous frequencies.
The advantage of this method is that all the non-linearites in the system of study are represented. Also, amplitude of the oscillations can be observed for different signals such as power, voltage and torque, as well as the speed with which these oscillations grow.
One disadvantage is that due to the high level of details required to model the controls and the mechanical system, it could be cumbersome to model large systems.

### 3.3.2 Eigenvalue (Modal) Analysis

This is one fundamental method to analyse the system. It requires that the complete system of study be represented by its linear differential equations and then a state-space model can be obtained for it as follows. Then, the eigenvalues of the system can be obtained. They provide information about the frequencies of natural oscillations of the system and also the damping of these frequencies (modes) [9]. Different eigenvalues sets could be obtained by changing the different control settings or operation conditions and then noticing the movement of the eigenvalues which gives an idea about the effect of these changes in the system stability.
The advantage of this approach is that not only does it provide information about the oscillatory modes, but also about how much damping the system presents for those modes. However, a major disadvantage of this method is that it requires detailed mathematical representation of the system in order to obtain its state-space model [9].

### 3.3.3 Frequency Scanning

For this method, simulation is used to compute the impedance of the network seen from the generator bus of interest, i.e. by looking into the network along the whole sub-synchronous frequency range. The result is the spectrum of the impedance (real and imaginary) along the sub-synchronous range.This approach is mainly for a preliminary study of the sub-synchronous oscillations [19]. Oscillations due to induction generator effect at a specific frequency is expected if the network resistance is negative and the inductance is zero. This method also provides information about

suspected torsional interaction and transient torque [25].
The advantage of this approach is that it gives a quick estimate of the risk of SSR for different contingencies in the network [8]. However, for the study of TI, other methods are necessary to evaluate its risk such as damping torque analysis [9].

## 3.4 Wind Farms Vulnerability to Sub-synchronous Resonance

In chapter 2 the different types of wind turbine generators were introduced. In this section, the susceptibility of the 4 types to SSR with series-compensated lines will be briefly presented.

### 3.4.1 Type-1 (Fixed-speed)

Type-1 wind power plant was found not to show sub-synchronous instability. This can be attributed to the simple nature of this type of plant as it does not contain any power electronics drive, which is the main cause of the sub-synchronous negative resistance [5].

### 3.4.2 Type-2 (Limited variable-speed)

At a certain compensation level, sustained sub-synchronous oscillations were noted in the active power from the wind farm. These oscillations were noted to be almost zero with lower compensation level.

### 3.4.3 Type-3 (DFIG-based)

Unstable oscillation were noticed in case of this type. These oscillations have different frequencies depending on the compensation level, output power and DFIG controller parameters. [5][22]

### 3.4.4 Type-4 (Full-converter)

It was reported that this type of wind generators did not show SSR with series compensated lines. [24].

## 3.5 First SSCI Incident in DFIG installation

The first SSCI incident was between a 150 MW DFIG-based wind farm and a 345 kV series-compensated transmission line. Fig. 3.1 shows part of the network, which includes a 200 MW DFIG-based wind farm that feeds the series-compensated line between Nelson Sharpe and Rio Hondo. The connection point is at Ajo. This line, at the time of incident, was at 50% compensation level. In October 2009, a single-line-to-ground fault occurred at the 37 miles-long line between Ajo and Nelson Sharpe. The fault resulted in tripping this line after 41 ms (2.5 cycles), which rendered the wind farm radially connected to the series-compensated line between Ajo and Rio Hondo. The new compensation level (after clearing the fault) became 90% (a very high level).

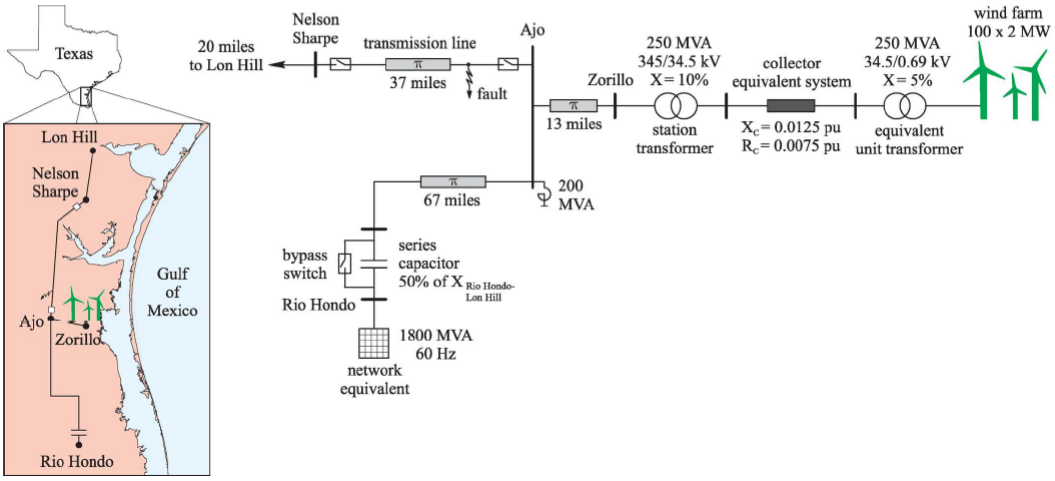


**Figure 3.1:** Part of the south Texas network which experienced the first SSCI in 2009 (Courtesy of Andres Leon [2])

As a result of this configuration, rapid sub-synchronous oscillations (around 20 Hz) in voltage and current started to build up. In 1 second, the voltage level reached almost 2 pu while the currents recorded reached 4 p.u as shown in Fig. 3.2.

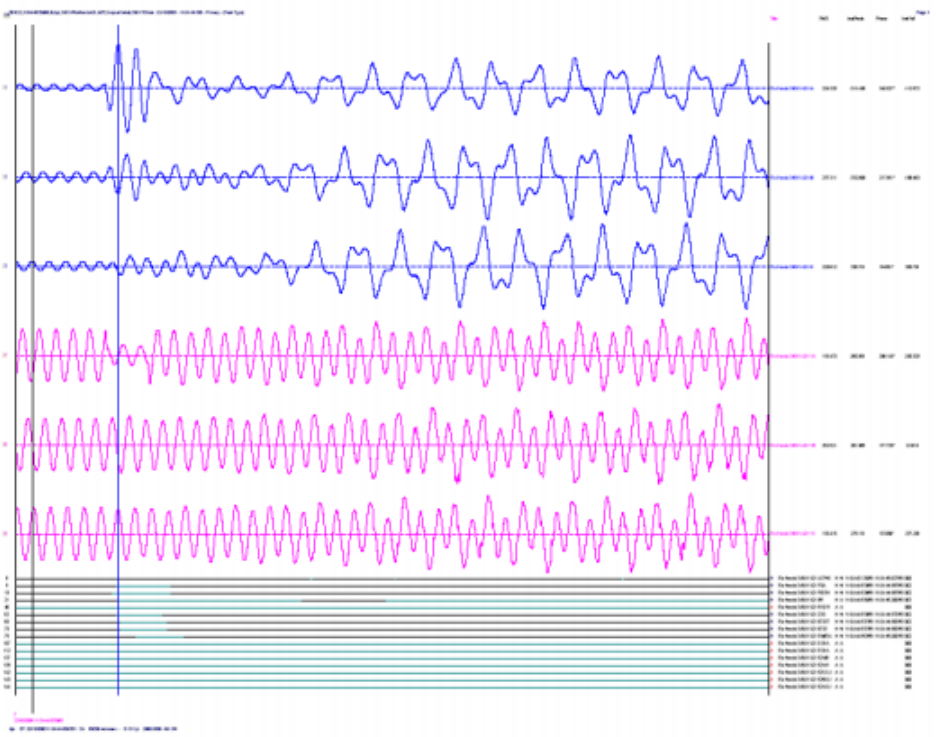

**Figure 3.2:** Field recordings of the first SSCI incident at Ajo representing from top: line currents to Rio-Hondo (phases a, b, and c in blue) and phase voltages in phases a, b and c (in pink) [22]

During the event, a number of wind turbines entered crowbar state. Also, the series capacitor was bypassed.

## 3.6 Damping of Sub-Synchronous Oscillations using shunt FACTS

Both series and shunt FACTS devices have been used to mitigate the SSI in power systems. Shunt devices include SVC (Static Var Compensator) and STATCOM (STATic synchronous COMpensator). SVC in essence is a TCR (Thyristor Controlled Reactor) and a TSC (Thyristor Switched Capacitor) along with a fixed capacitor while STATCOM is a VSC (Voltage Source Converter). Both deviices are used to dynamically inject or absorb reactive current at the point of connection. As for series devices they include: TSSC (Thyristor-Switched Series Capacitor), TCSC (Thyristor-Controlled Series Capacitor) and SSSC (Static Synchronous Series Compensator). The focus in this thesis will be on the shunt devices.
Table summarises some of the approaches in the technical literature for damping different types of SSO using shunt-connected FACTS devices. This summary is taken from papers: [27],[28],[13],[12]

**Table 3.1:** SSR damping using shunt FACTS

| Application | Device size | Control signal | Main Feature |
|---|---|---|---|
| SSR for Synch. Gen. | SVC @ Generator bus | Mach. volt. & speed | Optimal tuning of PI controller |
| SSR for Synch. Gen. | SVC (38 %)@ Midpoint | Speed deviation | Washout filter + PD ctrl. |
| TI for SEIG Wind Farm | SVC (60 %) @ Windfarm bus | Speed deviation | Washout filter + P ctrl. |
| SSCI with DFIG Wind-farm | FC(15%)+ SVC (11%) Wind-farm bus | Line power | Gain+ Washout filter+ Lead-lag comp.+ Gain adaptation |
| SSCI with DFIG Wind-farm | STATCOM(11%) @ Wind-farm bus | Rotor speed | Gain+ Washout filter+ Lead-lag comp.+ Gain adaptation |

Where SEIG stands for Self-Excited Induction Generator, DCIM for: Double Cage Induction Motor and FC for: Fixed Capacitor.

## 3.7 Summary

In this chapter the concepts of sub-synchronous resonance (SSR) and sub-synchronous interaction (SSCI) were introduced. Next, the methods used for SSI analysis were discussed flollowed by the vulnerability of the different types of wind generators to SSI. After that, a brief description of the first SSCI incident isgiven. Finally, a literature review of the methods used for damping SSR using shunt FACTS devices and a comparison among methods istabulated.

# 4

# Proposed Methodology

This chapter presents the methodology used in this thesis for both the analysis and mitigation of the sub-synchronous resonance caused by the interaction a of DFIG controller with a series-compensated network. The first section will introduce the network used for the study in addition to the frequency scan technique and the positive net damping method used for stability analysis. The second section will introduce the methods here proposed to detect the presence of sub-synchronous components in the active power signal. Then, it will proceed to estimating the frequency of the detected sub-synchronous components followed by the approach used to track a specific component. The chapter concludes with a short summary.

## 4.1 Analysis of sub-Synchronous resonance in DFIG farms

### 4.1.1 Study system

***Network:***

For the study of the sub-synchronous resonance phenomenon, the IEEE First benchmark model (FBM) for computer simulation of sub-synchronous resonance is here used. The model is originally developed to study SSR between a series-compensated network and the mechanical system of the Navajo project. The rotor is represented by a multi-mass spring mass model for the mechanical dynamics. The electrical network is a simple RLC network, which represents a transmission line connected to an infinite bus as in the Figure 4.1.

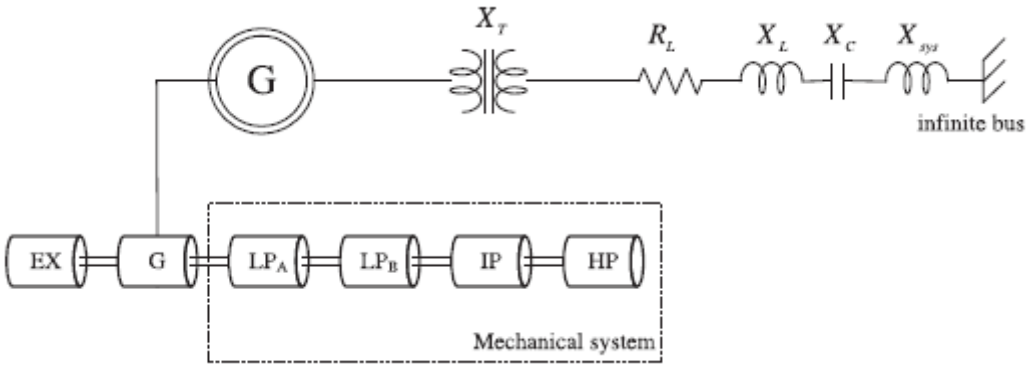


**Figure 4.1:** The IEEE original FBM for SSR studies [8]

The data of the original system are listed in Table 4.1.

**Table 4.1:** IEEE FBM Network Parameters

| | | |
|---|---|---|
| Network resistance | $R_L$ | 0.02 |
| Transformer reactance | $X_T$ | 0.14 |
| Transformer ratio | | 26/539 kV |
| Line reactance | $X_L$ | 0.5 |
| System reactance | $X_{sys}$ | 0.06 |

It is clearly noticeable that this system has to be modified for the purpose of DFIG studies. The synchronous generator and its mechanical system in Figure 4.1 has to be replaced by an equivalent DFIG wind farm as in Figure 4.2 in addition, a parallel transmission line is connected to the transformer in order to make sure that the system is stable initially and then create the instability by removing this line.

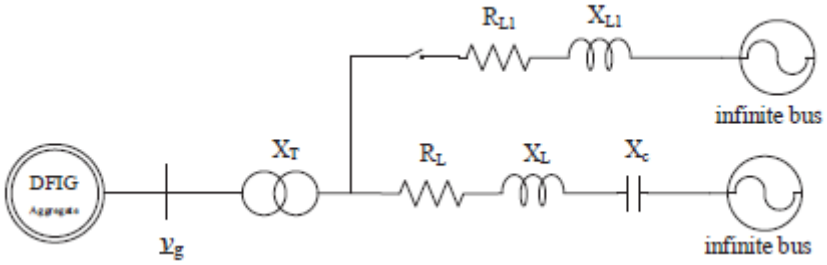


**Figure 4.2:** The IEEE modified FBM for SSR studies [29]

### *DFIG wind farm*

The wind farm is modelled in PSCAD/EMTDC as a 2.6 MVA generator. In order to include only the electrical dynamics, the mechanical prime mover of the DFIG is represented by a single-mass mechanical system. Table 4.2 lists the generator's parameters.

**Table 4.2:** DFIG generator parameters

| | | |
|---|---|---|
| Base power | $S_{base}$ | 2.6 MVA |
| Base voltage | $V_{base}$ | 0.69 kV |
| Stator leakage impedance | $X_{ls}$ | 0.179 |
| Magnetizing inductance | $X_M$ | 4.38 |
| Wound rotor leakage inductance | $X_{lr}$ | 0.0737 |
| Stator resistance | $R_s$ | 0.0105 |
| Wound rotor resistance | $R'_r$ | 0.00856 |
| Second line resistance | $X_f$ | 0.2 pu |
| Second line resistance | $R_f$ | 0.01 pu |
| Second line resistance | $C_{dc}$ | 3.5 pu |

Since the windfarm to be studied has a 892.4 MVA size, a scaling transformer is used. It is available in the ETRAN library for PSCAD and it is shown in Figure 4.3. This transformer scales up the power by using the specified the current scaling factor (scale).

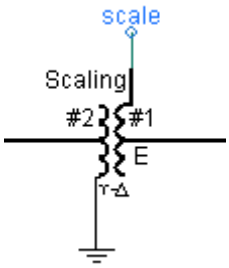


**Figure 4.3:** ETRAN component: Scaling transformer

### 4.1.2 Time-domain analysis

The triggering event for the SSCI is the disconnection of the upper branch depicted in Figure4.2. This event renders the DFIG power plant radially connected to the series compensated network. This situation resembles the case in the Zorillo wind farm incident in 2009 [2]. After the application of the contingency, sub-synchronous resonance is noticeable on the signals of the active power, voltage and current as in Figure **??**. From the figure, clear instability is noticed after the breaker is opened after 3 seconds of simulation. Signals of active power and RMS voltage show unstable behaviour as they start to oscillate and grow with a sub-synchronous frequency. Also, the current signal shows sub-synchronous behaviour as its amplitude is modulated in a growing manner.

Fig 5.6 shows the implementation of the study system in PSCAD/EMTDC, which is used for both time domain and frequency domain analysis.

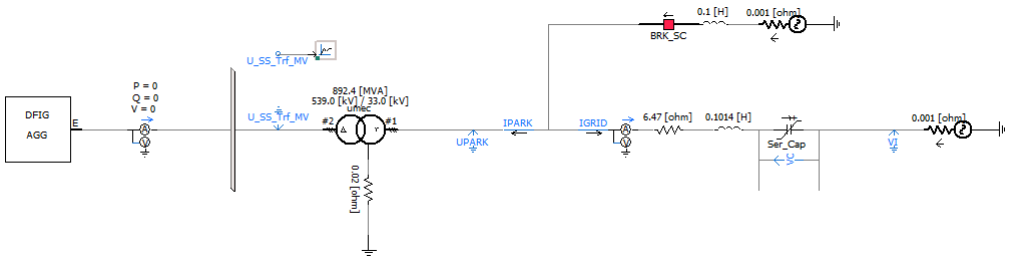


**Figure 4.4:** Screen print of the used IEEE FBM model

To study the effect of different parameters on the system's vulnerability to SSCI, the following aspects are considered:

- Series compensation level: which changes the resonance frequency of the electric network. This is done by simply changing the value of the series compensator capacitance.

- Wind farm output power: To test the effect of different power set-points on the possibility of SSR and on the frequency of SSR.

- DFIG controller parameters: Previous studies [2] [18] [22] [29] show that change in the parameter of the PI controller of the RSC current controller greatly affects the stability of the DFIG and hence the presence of SSCI. In order to do this, the current controller bandwidth controller is changed. In order to include only the effect of the RSC control system, the GSC is disconnected from the network and an ideal large voltage source is placed at the DC link between the RSC and GSC.

### 4.1.3 Frequency-domain Analysis (Nyquist criterion)

#### *Positive net-damping stability criterion*

This method is based on the study of the overall system using the input impedance of the DFIG. The idea is based on treating both generator and network as single-input single-output (SISO) systems, which allows obtaining a feedback system of both generator and network as in Figure 4.5.

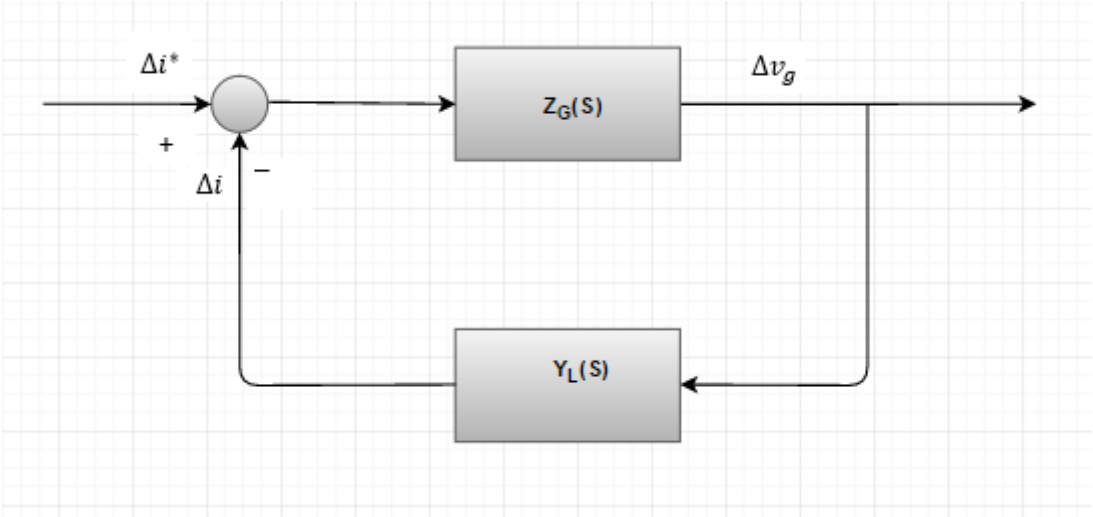


**Figure 4.5:** Closed loop system of the DFIG impedance and the series-compensated transmission admittance (In frequency domain)

In the figure, $Z_G$ is the impedance of the DFIG seen from its stator terminal and $Y_L$ is the series-compensated transmission line admittance seen from the point of connection to the DFIG. This representation allows the application of Nyquist criterion for stability on the open loop transfer function $Z_G Y_L$ [29].

In order to apply this method of analysis, it is essential to obtain the impedance of the DFIG farm as a function of frequency using the impedance-frequency scan method explained in the next section. Also, the impedance (or admittance) of the transmission network can be obtained as below.

$$Z_G(j\omega) = R_G(\omega) + jX_G(\omega) \tag{4.1}$$

$$\frac{1}{Y_L(j\omega)} = R_L(j\omega) + jXL(\omega) \tag{4.2}$$

where $Z_G$ is the aggregate DFIG farm impedance ($R_G$ and $X_G$ are the real and imaginary parts) and $Y_L$ is the transmission network admittance ($R_L$ and $X_L$ are the real and imaginary parts of the network impedance).
For the open-loop transfer function $Z_G Y_L$ is expressed as following (substituting $S$ with $j\omega$)[29]:

$$\begin{aligned} Z_G(\omega)Y_L(\omega) &= \frac{R_G(\omega) + jX_G(\omega)}{R_L(\omega) + jX_L(\omega)} \\ &= \frac{R_G(\omega)R_L(\omega) + X_G(\omega)X_L(\omega)}{R_L^2(\omega) + X_L^2(\omega)} + j\frac{R_L(\omega)X_G(\omega) - R_G(\omega)X_L(\omega)}{R_L^2(\omega) + X_L^2(\omega)} \end{aligned} \tag{4.3}$$

In order for the open-loop transfer function to be asymptotically stable, the Nyquist curve must not encircle -1. In order to apply this in Eqn. 4.3, then the imaginary

part is set to zero. Then, denoting the resonance frequency as $\omega_{res}$, the following applies: $R_L(\omega_{res})X_G(\omega_{res}) - R_G(\omega_{res})X_L(\omega_{res}) = 0$, which gives:

$$\frac{X_L(\omega_{res})}{X_G(\omega_{res})} = \frac{R_L(\omega_{res})}{R_G(\omega_{res})} \tag{4.4}$$

Substituting Eqn. 4.4 in Eqn. 4.3 gives:

$$Z_G(j\omega_{res})Y_L(j\omega_{res}) = \frac{R_L(\omega_{res})}{R_G(\omega_{res})} \tag{4.5}$$

If Eqn. 4.5 is larger than -1 i.e. $R_L(\omega)/R_G(\omega) > -1 \Rightarrow \mathrm{R}_L(\omega) + R_G(\omega) > -1$, then the Nyquist curve will not encircle -1. [16]
Thus, the criterion for this particular transfer function is obtained by the condition [29]:

$Re[Z_G(j\omega)Y_L(j\omega)] > -1$ and $Imag[Z_G(j\omega)Y_L(j\omega)] = 0$

***DFIG Impedance-Frequency scanning***

To obtain the above mentioned $Z_G(s)$ for the DFIG, an impedance scan needs to be implemented for the DFIG model in PSCAD. This scan gives values of both real and imaginary part of the DFIG impedance for the whole frequency spectrum of interest. The DFIG is a non-linear system, so to obtain the impedance at a certain frequency by simulation, one way is to excite the DFIG by injecting 3-phase currents (or voltages) into the stator terminal at the required frequency, and then measuring the response of the generator in terms of voltage (or current). For the measured signal, an FFT is performed in order to obtain its magnitude and phase at the desired frequency. This process is repeated for the whole frequency spectrum required, which is the sub-synchronous range in our case (below 50 Hz). Figure 5.1 shows the implemented system in PSCADEMTDC for DFIG-side impedance-frequency scanning.

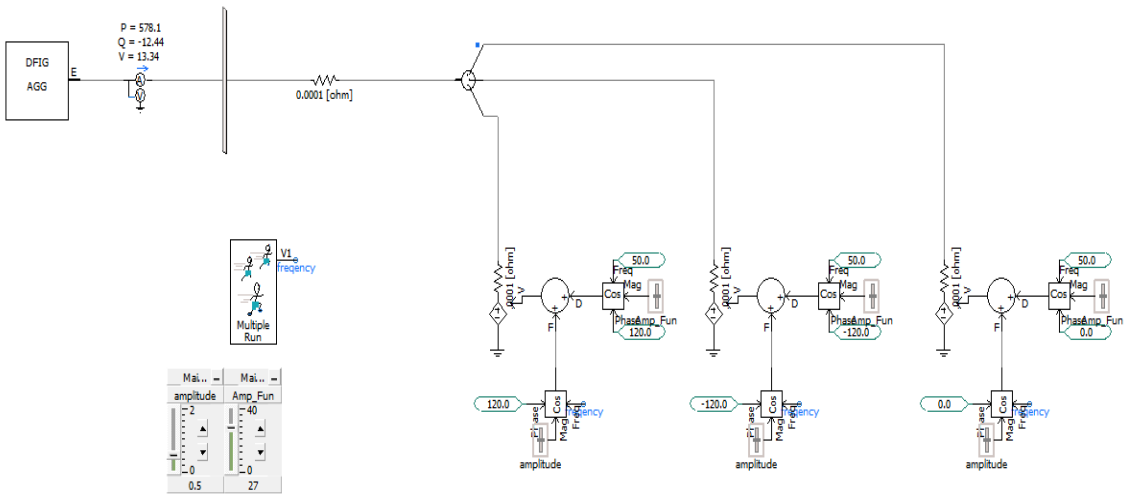


**Figure 4.6:** Implemented impedance-frequency scanning for DFIG

## 4.2 STATCOM voltage control [8]

Figure 4.7 summarises the voltage control strategy of the STATCOM. It relies on vector control which allows independent control of both active and reactive currents (consequently active and reactive power). The main component in the system is the Voltage-Source Converter (VSC), which is a converter that has a DC-Link capacitor on its DC side and IGBT valves. The valves are switched between On and Off states by Pulse Width Modulation (PWM) technique, which is represented by the PWM block in Figure 4.7. Under steady-state condition and with very high switching frequency of the PWM, the VSC can be modelled as a voltage source.
In order to implement the control system in dq-coordinates, all the measured quantities (bus voltage and line current) need to be transformed into *dq*-system using the *abc/dq* block in the figure. This coordinate system rotates with the frequency of the grid, however, it needs to be aligned to the grid voltage vector in order to obtain DC quantities of the *d*- and *q*- components. In order to align the coordinate system to the grid voltage, the control system needs to know the voltage vector angle which is performed using a Phase-Locked Loop (PLL). The PLL estimates the instantaneous angle $\theta$ of the voltage vector, which is further used by the *abc/dq* block to obtain the proper *d*- and *q*- components of the line current. In these applications, the voltage vector is aligned to the *d*-axis during steady-state.This implies that the *d*-component of the voltage vector equals the RMS values (using power invariant transformation) while the q-component equals to 0 (in steady-state). Thus, the active component of the current is the d-component while the *q*-component is the reactive one.
Finally, in order to control the STATCOM terminal voltage, two Proportional-Integral (PI) control loops are used. The proportional gain of the controller allows for reference tracking while the integral gain is used to remove steady-state errors due to different reasons such as measurement noise and non-linearity.
Now, the control strategy can be summarised as follows:

1. Measurement and sampling of the grid voltage and line currents ($\underline{e}(t)$ and $\underline{i}(t)$).

2. Transform those quantities to the synchronised rotating *dq*- system, which is achieved by first transforming the 3-phase quantities to fixed 2-phase coordinate system ($\alpha$ $\beta$) and then move to the rotating *dq*- system using the transformation angle $\theta$ from the PLL block.

3. The error between the measured voltage and the reference voltage is used as input to the PI reactive power controller, which produces a reference for the reactive (*q*-) current that is used to produce a *q*-current error signal, which is used further as an input to the current controller that produces the reference signal to the PWM block.

4. The PWM calculates the duty-cycles of the converter and passes the switching signals to the VSC valves hence producing the desired voltage reference at the connection bus.

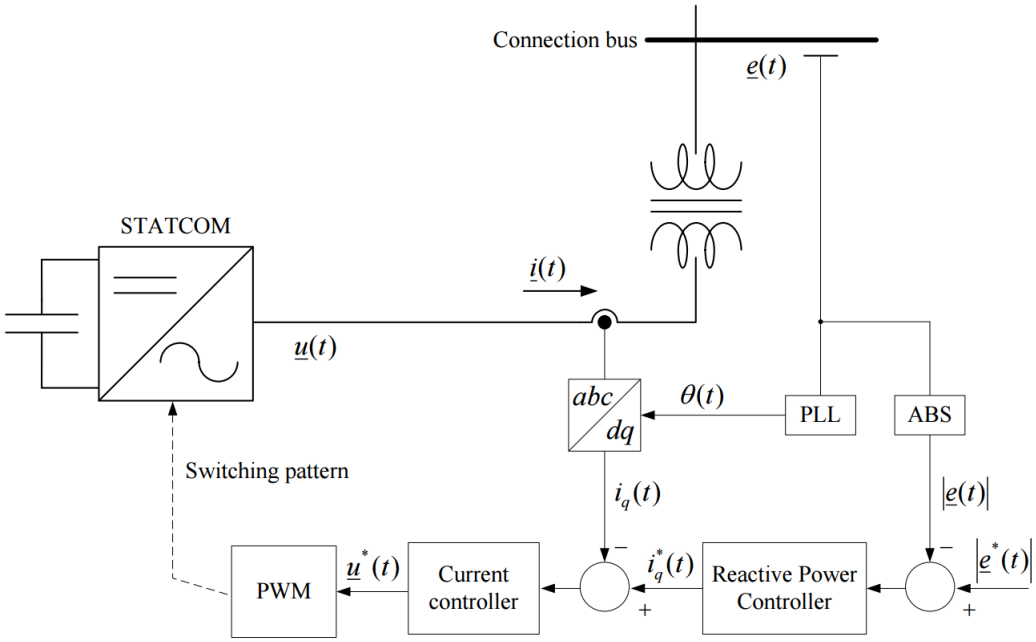


**Figure 4.7:** STATCOM voltage control [8]

## 4.3 Control Strategy of a STATCOM for SSCI Mitigation

In order to solve the problem of SSCI by increasing the system's damping, it is important to know that these oscillations occur under the following conditions:

1. The presence of a DFIG wind farm which presents negative resistance along almost the whole sub-synchronous frequency range.

2. The presence of a series compensated transmission line electrically near the concerned DFIG wind farm: this creates the electrical resonance condition (not necessarily unstable).

3. The sum of the damping (resistance) of both the network (as seen from the generator side) and generator (as seen from the network side) is less than zero according to [16], which renders the resonant oscillations in growing and not facing any damping in the system.

4. The frequency of oscillations is the frequency at which the sum of those two resistances is equal to zero (which depends basically on the network )

According to the IEEE PES Wind Plant Collector System Design Working Group in [3], a 100-MVAR STATCOM provides sufficient reactive power compensation for a 200 MW wind power plant. This STATCOM will be used to support for reactive power during normal operations and also to improve the stability of the system during SSR conditions. For this purpose, a supplementary controller is developed and

added to the STATCOM voltage control. This supplementary controller is expected to drive the STATCOM during the SSR conditions so that it damped these oscillations.
A major issue in the SSCI due to DFIG is that actually the frequency of the oscillations is not known since the DFIG wind farm presents negative resistance for almost the whole sub-synchronous range. This implies that oscillations occur at a certain frequency only if the electrical damping (resistance) of the network at resonance frequency is small compared to the magnitude of DIFG resistance at that frequency.
The proposed control strategy involves four steps:

1. Detection of sub-synchronous current components in the output of the DFIG wind farm.

2. Estimation of the frequency of the detected component.

3. Extraction the component of this frequency in the active power signal.

4. Use of this component -after multiplying it by a gain-to modulate the voltage reference signal in the STATCOM control in order to damp the oscillations.

### 4.3.1 Online detection of sub-synchronous components

A major issue in the problem of SSR damping is the detection of sub-synchronous components in the output current of the wind farm. Available approaches to achieve this purpose are based on frequency analysis [1][6]. These methods require storage of signals and then to apply the analysis method to it, which is not acceptable in our application because of the high speed of SSO build up. Hence, information about the SSR need to be available online.
Abhisek Ukil in [33] suggests an approach for detecting sub-synchronous components in a sinusoidal signal on-line. The approach is based on detecting the envelope of the signal measured. Below is the summary of the method.

***Assumptions:***

Let us assume that the components that are to be detected are of sub-synchronous nature and that they are sinusoidal.

***Mathematical proof***

Let us assume a fundamental sinusoidal signal

$$f_f = Asin(\theta) \tag{4.6}$$

where $A$ is the signal amplitude and $\theta$ is its angular frequency. Let us also assume the presence of a disturbance signal

$$f_d = Bsin(k\theta) \tag{4.7}$$

where B ($\neq$ A) is the disturbance amplitude and k ($\neq$ 1) is a multiplication factor. The total signal is then

$$f = f_f + f_d = Asin(\theta) + Bsin(k\theta) \tag{4.8}$$

Here, the peak signal is considered. In order to take peak in consideration (both positive and negative peaks), the following condition is assumed:

$$\frac{df}{d\theta} = Acos(\theta) + Bkcos(k\theta) = 0 \tag{4.9}$$

Now, applying Eqn. 4.9 to $A^2 = A^2sin(\theta) + A^2cos(\theta)$, the following is obtained:

$$\begin{aligned} Asin(\theta) &= \sqrt{A^2 - A^2cos^2(\theta)} \\ &= \sqrt{A^2 - B^2k^2cos^2(k\theta)} \\ &= \sqrt{A^2 - B^2k^2 + B^2k^2sin^2(k\theta)} \end{aligned} \tag{4.10}$$

Replacing Eqn. 4.10 into Eqn. 4.8 gives the expression for the peak of the whole signal:

$$f_{peak} = \sqrt{A^2 - B^2k^2 + B^2k^2sin^2(k\theta)} + Bsin(k\theta) \tag{4.11}$$

Looking at Eqn. 4.11 it can be noticed that it includes the information of the disturbance. If this disturbance frequency is sub-synchronous (i.e. $k < 1$) and its amplitude is less than that of the fundamental ($B \leqslant A$), then the term ($B^2k^2sin^2(k\theta)$) can be neglected, thus giving this approximate term:

$$\hat{f}_{peak} \approx \sqrt{A^2 - B^2k^2} + Bsin(k\theta) = d + Bsin(k\theta) \tag{4.12}$$

where $d$ is an offset, which means that this signal represents the disturbance since $A, B$ and $k$ are constants. The signal in 4.12 will be periodic if the disturbance is maintained. Thus, the envelope of the voltage (or current) can be estimated to indicate the presence of a sub-synchronous components.

***Envelope detection method***

The typical diode circuit is to detect the envelope of a sinusoidal signal is the circuit shown in Figure 4.8

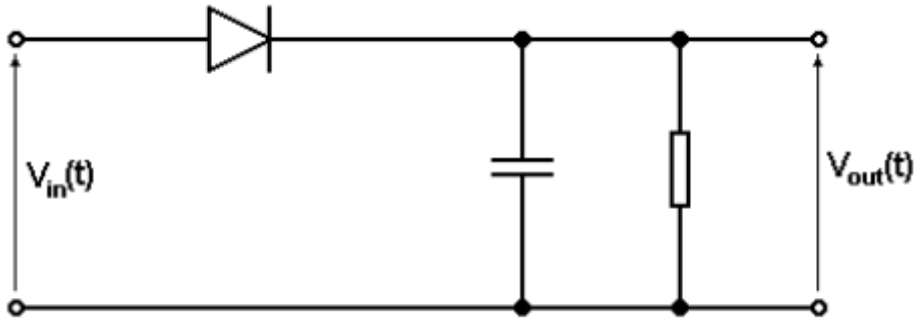


**Figure 4.8:** Typical electronic circuit for envelope detection

where $V_{in}(t)$ represents the disturbed sinusoidal signal and $V_{out}(t)$ is the envelope of that signal. In this circuit, the diode allows current only in the positive half of the input signal while the capacitor stores the charge during the rising part of the input signal and discharges it slowly during the falling part.
Figure 4.9 shows the tracking of the envelope (in red) of the signal (in blue).

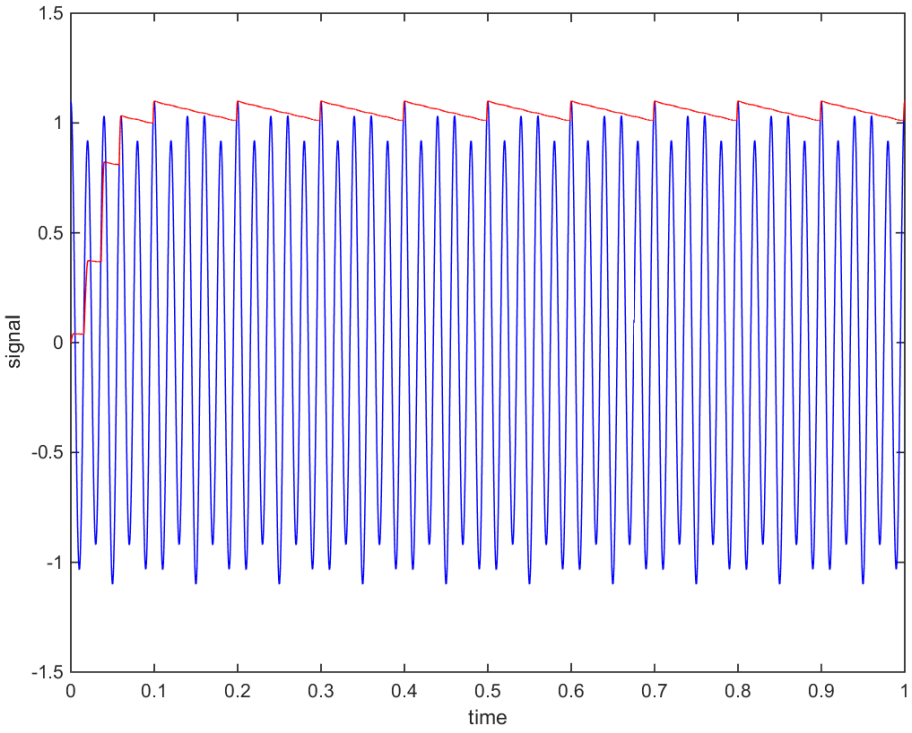


**Figure 4.9:** Envelope detector output using the diode detector

The problem with this method is that is has sharp transition from the bottom of the envelope to its top. This sharp transition gives undesired spikes when the derivative og the envelope is taken later on. A more convenient method for envelope detection is by squaring and low-pass filtering of the signal [23]. This gives a smoother envelope signal as shown in Figure 4.11. Figure 4.10 shows the implementation of the detector in PSCAD.

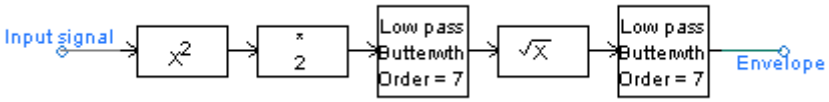


**Figure 4.10:** Envelope detector implementation in PSCAD

Figure 4.11 demonstrates the use of the envelope detector, where the upper figure shows the voltage of the wind farm and the SSCI is triggered at time=0.5 s. The presence of SSR modulates the signal as seen in the top figure. The middle figure shows the extraction of the envelope while the bottom one shows both signals together.

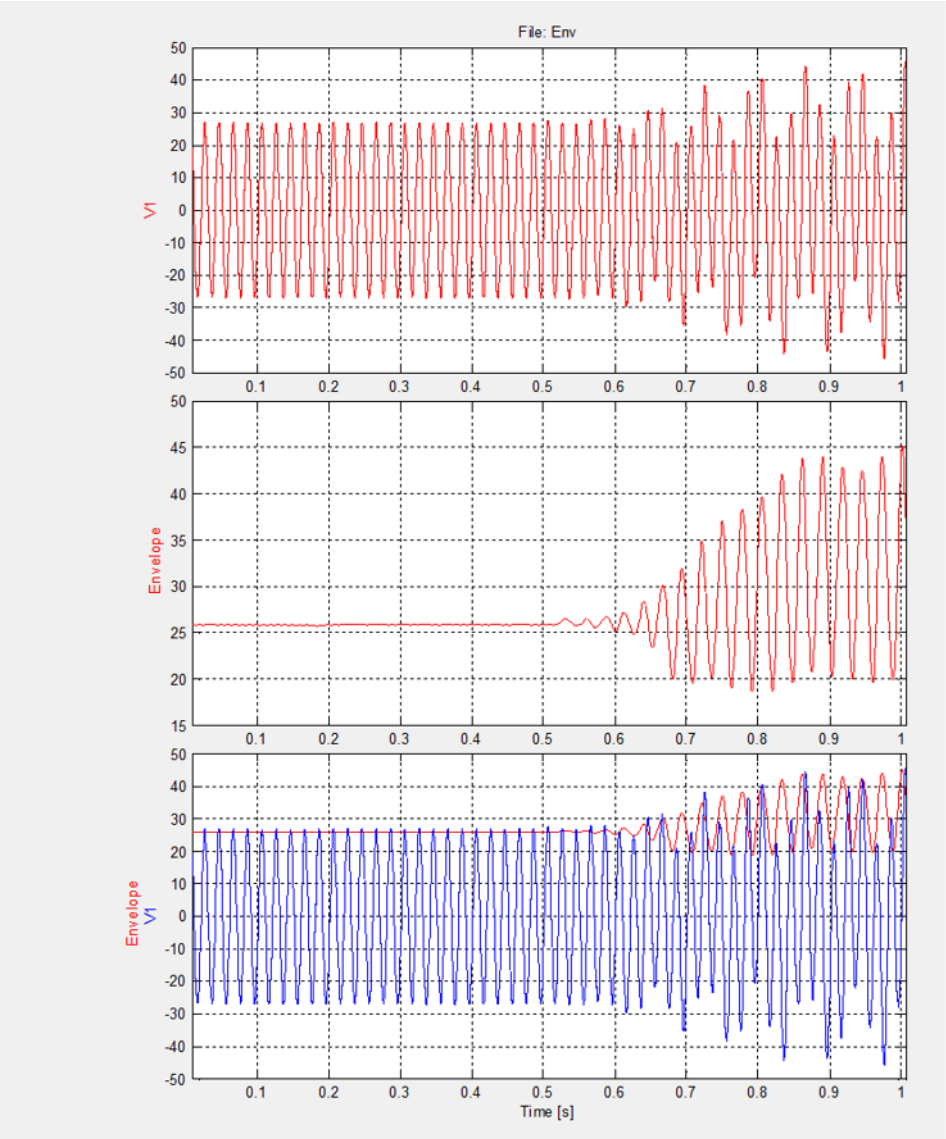


**Figure 4.11:** Detection of envelope of a distorted signal

It is to be noted that the first low pass filter has a cut-off frequency of double the fundamental frequency (100 Hz in our case) since the squaring doubles the frequency. The second filter's cut-off frequency is 45 Hz (the typical upper limit of the sub-synchronous range).

### 4.3.2 Frequency estimation

After detecting the presence of sub-synchronous components, it is now possible to estimate its frequency.
A simple method of zero-crossing detection is used, but before that it is necessary to obtain the derivative of the envelope. The reason behind this is that under normal conditions, the envelope is a d.c. signal (greater than zero), so it is not possible to get zero-crossing for it. However, differentiating allows to set the offset to zero so that when the oscillations appear, it would be possible to apply a zero-crossing detection method.

### 4.3.3 Extraction of sub-synchronous components

After detecting the presence of a sub-synchronous component in our signal and then estimating its frequency, it is time now to extract it from a measure quantity to be used as a control signal. The control signal selected here is the real power output of the DFIG wind farm since it includes all the information of both voltage and current at the terminal of the wind farm.
Different methods are available to perform this task. A very common one is the method of cascaded filter links presented in [7], which employs three filters (washout, low pass and lead-lag compensator)to obtain the desired component of certain frequency.
In our case, another method which gives more accurate and higher selectivity of frequencies is used. It also gives a faster response as compared to the cascaded filters method. This method is based on the use of low pass filters [7].

#### *Mathematical proof*

The following is a mathematical demonstration on how the LPF method works.
Assuming that the signal used is active power, then it can be expressed as follows

$$p(t) = P_0(t) + P_{osc}(t) = P_0 + P_{ph}(t)cos(\omega_{osc}t + \phi(t)) \tag{4.13}$$

where $P_{osc}$ expresses the oscillatory power component. It is further expressed by its amplitude ($P_{ph}$), angular frequency ($\omega_{osc}$) and phase ($\varphi$).

The oscillatory active power term in 4.13 can be expressed as the phasor $\underline{P}_{ph} = P_{ph}e^{j\varphi}$ with an oscillation angle $\theta_{osc}(t) = \omega_{osc}t$, and then the measured power signal can be written as follows:

$$p(t) = P_0(t) + Real[\underline{P}_{ph}(t)e^{j\theta_{osc}}(t)] = P_0(t) + \frac{1}{2}P_{ph}(t)e^{j\theta_{osc}}(t) + \underline{P}^*_{ph}(t)e^{-j\theta_{osc}}(t) \tag{4.14}$$

Considering that $P_0$ and $\underline{P}_{ph}$ are slowly varying signals, then it can be concluded that Eqn. 4.14 contains three frequencies: 0, $\pm\omega_{osc}$. Now, applying low-pass filter to 4.14 it is possible to obtain estimations for the signals: $P_0$, $\underline{P}_{ph}$ , and $P_{osc}$ as follows:

$$\tilde{P}_0(t) = H_0[p(t) - \tilde{P}_{osc}] \tag{4.15}$$

$$\tilde{P}_{ph} = H_{ph}[2p(t) - 2\tilde{P}_0(t) - \underline{\tilde{P}}^*_{ph}(t)e^{-j\theta_{osc}(t)}]e^{-j\theta_{osc}(t)} \tag{4.16}$$

$$\tilde{P}_{osc} = \frac{1}{2}\underline{\tilde{P}}_{ph}(t)e^{j\theta_{osc}(t)} + \underline{\tilde{P}}^*_{ph}(t)e^{-j\theta_{osc}(t)} \tag{4.17}$$

where $H_0$ and $H_{ph}$ are the low-pass filter transfer functions for average and phasor extraction. The "Tilde" above any of the above represents an estimate of that quantity.

The two filters $H_0$ and $H_{ph}$ are selected to be low-pass filters with the following transfer function (in S-domain):

$$H_0(s) = H_{ph}(s) = \frac{\alpha_{LPF}}{s + \alpha_{LPF}} \tag{4.18}$$

In order to get the desired response, the cut-off frequencies of the two LPFs are selected to be smaller than the frequency of the oscillation (typically one tenth of it).
In order to get the frequency response of this controller, its state-space model is obtained according to [4] which has $p(t)$ as input and $P_{osc}$ as output as follows:

$$\frac{d}{dt}\begin{bmatrix}\tilde{P}_0\\ \tilde{P}_{osc}\\ \tilde{P}_\beta\end{bmatrix} = \begin{bmatrix}-\alpha_{LPF} & -\alpha_{LPF} & 0\\ -2\alpha_{LPF} & -2\alpha_{LPF} & -\omega_{osc}\\ 0 & \omega_{osc} & 0\end{bmatrix}\begin{bmatrix}\tilde{P}_0\\ \tilde{P}_{osc}\\ \tilde{P}_\beta\end{bmatrix} + \begin{bmatrix}\alpha_{LPF}\\ 2\alpha_{LPF}\\ 0\end{bmatrix}p(t)$$

$$\text{y}= \begin{bmatrix}0 & 1 & 0\end{bmatrix}\begin{bmatrix}\tilde{P}_0\\ \tilde{P}_{osc}\\ \tilde{P}_\beta\end{bmatrix} \tag{4.19}$$

Figure 4.12 shows two Bode plots obtained using the state-space model in 4.3.3 for two oscillation frequencies.

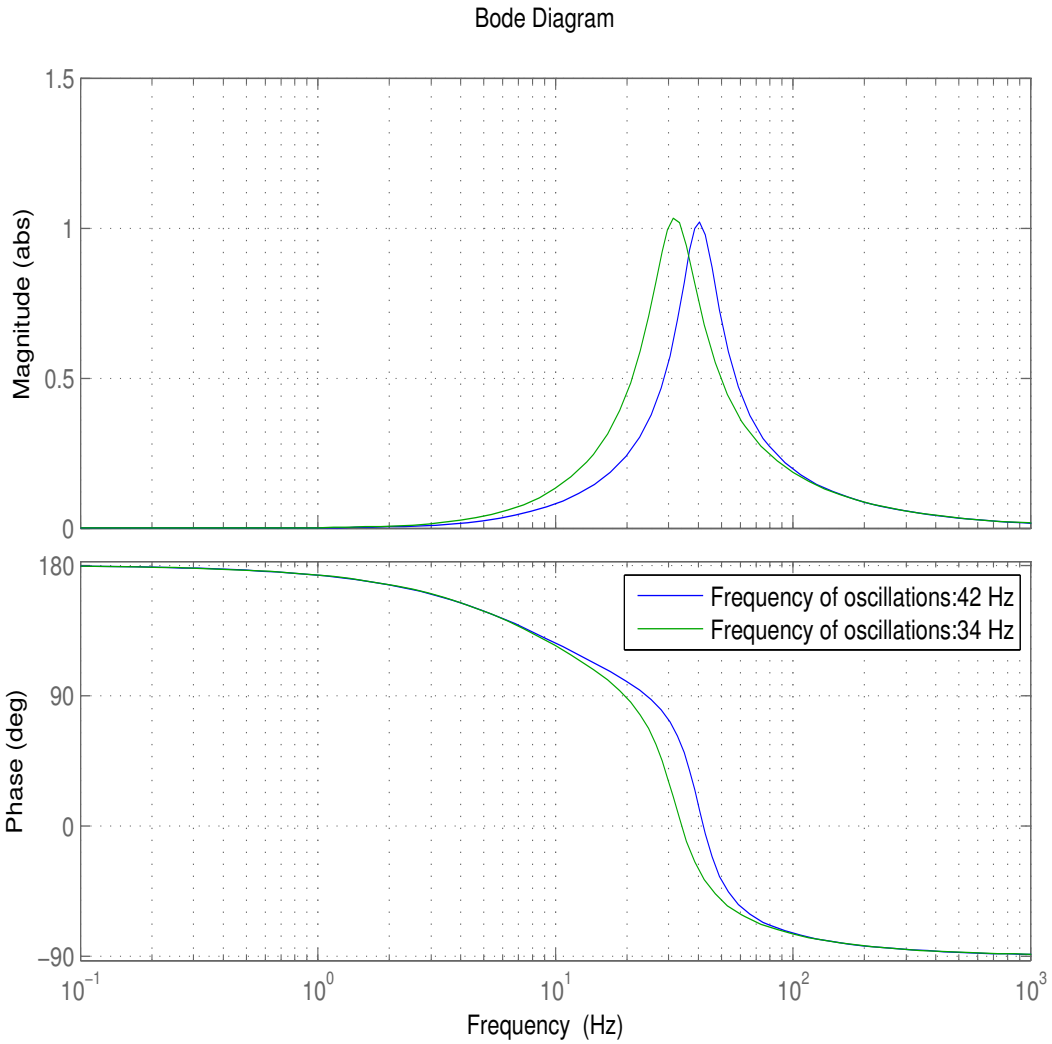


**Figure 4.12:** Bode plots of the low-pass filter method used to extract a signal with a certain frequency

Note that the transfer function has a gain of 1 at the required frequency while the phase shift at that frequency is 0 degrees. This attenuates the unwanted frequencies and outputs the signal of the desired frequency with a gain of 1.

#### 4.3.3.1 Overall STATCOM System for SSCI Mitigation

The following block diagram summarises the proposed control strategy for SSCI damping using a STATCOM.

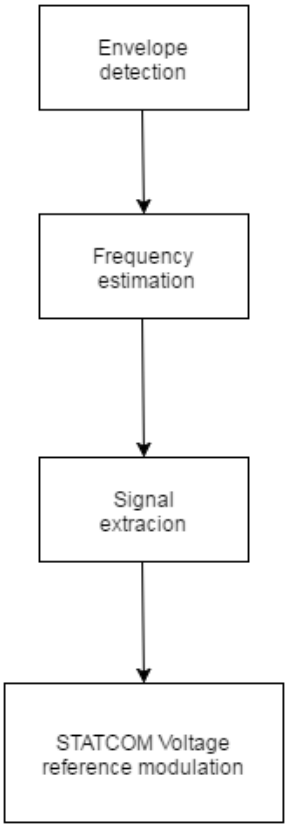


**Figure 4.13:** Control strategy of a STATCOM for SSCI damping

The first step is to detect the presence of an envelope on the instantaneous voltage signal of the DFIG wind farm. This envelope contains the information about the sub-synchronous components. In order to estimate the frequency of the envelope, it is passed through a differentiation block which outputs zero in the case of no sub-synchronous components. The zero crossing detection of the derivative is then used to estimate the frequency of the envelope. After estimating it, the frequency is next passed to the signal extraction block which tracks the power component of that frequency. This signal is further used, after a proper gain, to modulate the voltage reference of the STATCOM. This modulation adds the proper damping to the sub-synchronous power oscillations at the output of the DFIG wind farm.

### 4.3.4 Summary

In this chapter, the analysis and damping methodology is presented. The analysis method includes first obtaining the impedance-frequency scan of both the series-compensated network and the DFIG plant both seen from the PCC. This frequency scan gives an idea about how the DFIG impedance and resistance look like along the whole sub-synchronous frequency range. After that, the net-positive damping criterion and the Nyquist stability criterion can be applied. This method allows to evaluate the stability of the whole system graphically. To conclude, a novel control strategy is presented. It is based on detecting the presence of sub-synchronous com-

ponents and then accordingly modulating the voltage reference for the STATCOM.

# 5

# Case Studies

In this chapter, the results obtained from the proposed methodology are presented; first for the positive-net damping criterion using Nyquist method simulations and after for the time-domain simulations. For both approaches, different scenarios have been considered corresponding to different compensation levels, DFIG power outputs and DFIG controller bandwidths. The size of the wind farm is 892.4 MW while the size of the STATCOM used is 150 MVAR. For all of the simulations, the DFIG wind farm active power, voltage and line current are plotted.

## 5.1 Frequency-domain simulations

### 5.1.1 DFIG-side frequency-impedance scan

To gain insight on the DFIG impedance behaviour, impedance-frequency scan was performed on the DFIG wind-farm using PSCAD at its input as shown in 5.1 (block "DFIG AGG"). The idea is to apply 3-phase 50-Hz (fundamental frequency) voltage with the nominal voltage (33 kV RMS) and then modulate it with another small signal (about 5% of the nominal RMS) at different sub-synchronous frequencies in order to be able to obtain the harmonic impedance below the 50 Hz as shown in Fig. 5.1. The 33 kV rms is created by

The procedure is to run 49 cases with different frequency of the modulating signal (1 Hz step for each run) starting from 1 Hz and ending at 49 Hz. For each phase there is one DC source whose amplitude is controlled by a sum of two cosine signals: one is fixed at the fundamental frequency (50 Hz) with amplitude of 27 kV while the other cosine signal has amplitude of 1.35 kV and an incremental frequency at each run. This frequency is controlled by the "Multiple Run" block in Fig. 5.1. For each run, voltage is injected and it is recorded along with the DFIG current.After the DFIG reaches steady state (in terms of voltage and power), FFT (Fast Fourier Transform) is applied to both voltage and current signals and in order to obtain the harmonic impedance. Applying FFT means obtaining the magnitude and phase

of voltage and current at each frequency step, for example, for a frequency of 17 Hz: voltage is: $\mathrm{V}(17) = V(17)\angle\phi_V(17)$ while current is: $\mathrm{I}(17) = I(17)\angle\phi_I(17)$. The impedance at that frequency will be: $\mathrm{Z}(17)=\frac{\mathrm{V}(17)}{\mathrm{I}(17)} = \frac{V(17)\angle\phi_V(17)}{I(17)\angle\phi_I(17)}$

Distinct scenarios are studied to get knowledge about the behaviour of the DFIG impedance along the sub-synchronous range, for example for different power output levels and different current controller bandwidth values ($\alpha_{CC}$).

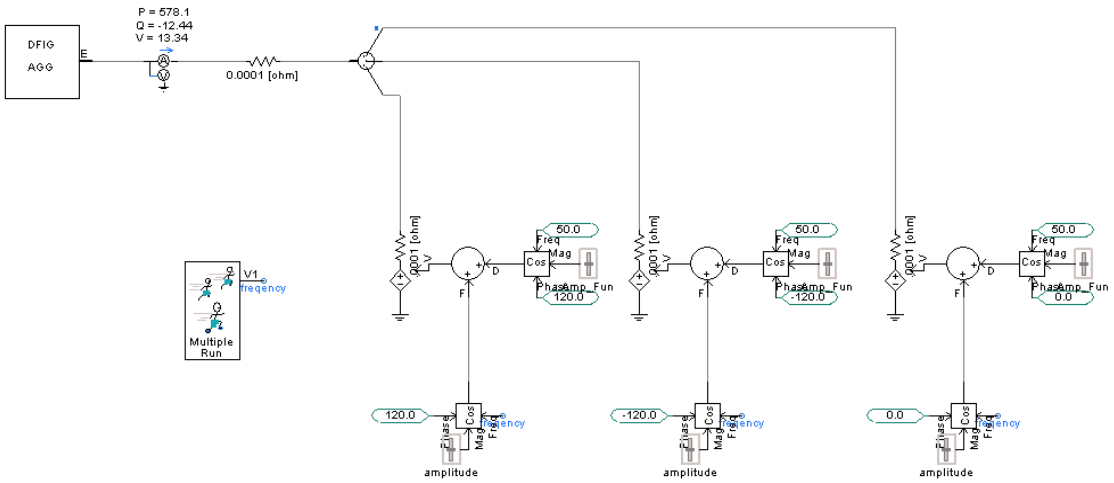


**Figure 5.1:** PSCAD setup used to perform the frequency of the DFIG wind farm

***Different power output levels***

Different operation conditions where simulated in terms of DFIG reference active power, which showed different behaviour of DFIG harmonic impedance as shown in Fig. 5.2. As depicted, the DFIG has more negative resistance at lower power output reference.

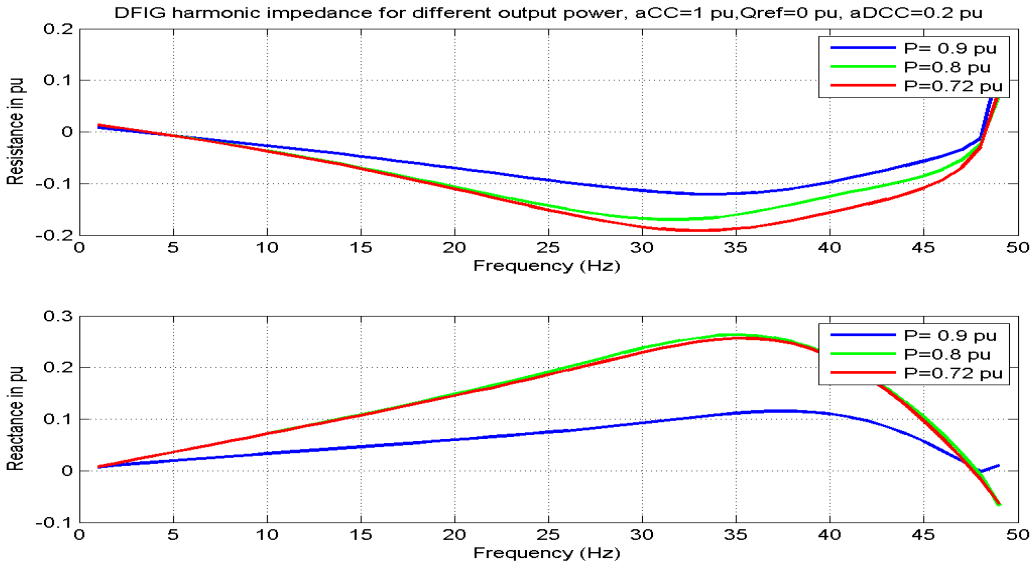


**Figure 5.2:** DFIG impedance scan: Different power output levels, $\alpha_{CC} = 1pu, Qref = 0pu$

The results indicate that for different power reference levels, the DFIG has different harmonic impedance. The lower the power is, the lower the resistance of the DFIG becomes. This means that for higher generation levels, the DFIG is less prone to SSCI since it would need less damping (resistance) from the system's side. The opposite happens when the generation level is lower, the DFIG resistance is more negative requiring the same amount and more of positive resistance from the grid side to avoid having SSCI condition.

### *Different current controller bandwidth* $\alpha_{CC}$

Different current controller bandwidths $\alpha_{CC}$ are used to investigate the effect of DFIG controller parameters in the generator's impedance. To do this, the reference power was fixed and only $\alpha_{CC}$ was changed. Fig. 5.3 illustrates the effect of the $\alpha_{CC}$ change on the generator's harmonic impedance.

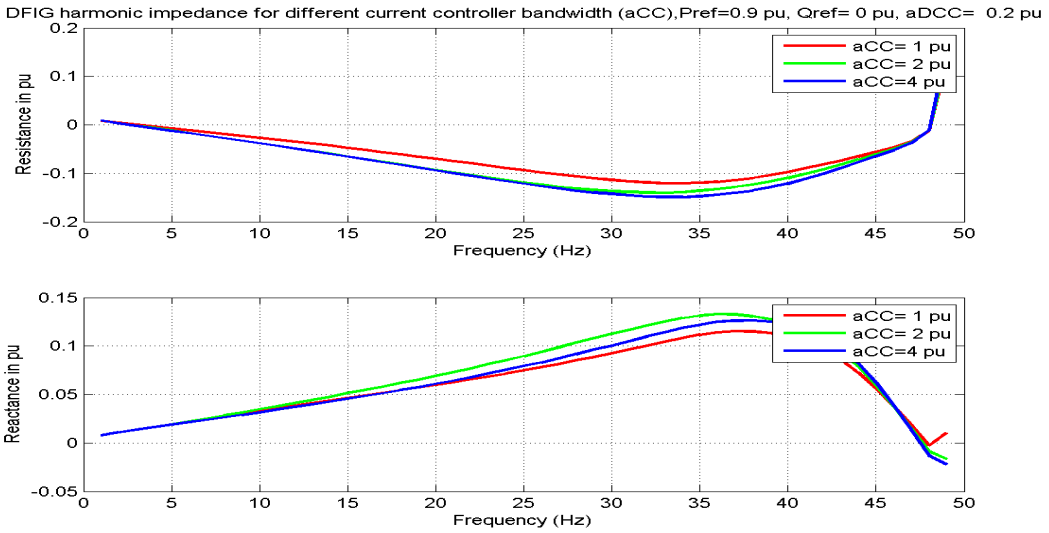


**Figure 5.3:** DFIG impedance scan: Different current controller bandwidth $\alpha_{CC}, Pref = 0.9pu, Qref = 0pu$

It can be noted that the higher the controller bandwidth is (faster controller), the more negative the DFIG resistance becomes. The lowest resistance is for $\alpha_{CC} = 4$ and the highest is for $\alpha_{CC} = 1$. This means that the faster the current controller is, the more damping (resistance) the DFIG needs from the network to achieve a net-positive damping and thus avoid sub-synchronous resonance.

### 5.1.2 Net positive damping criterion (using Nyquist stability criterion)

The Nyquist stability criterion described in section 4.1.3 was employed to investigate the effect of the different system's parameters on its stability. The criterion can be applied as follows: the system is unstable if the real part is smaller than (-1) when the imaginary part is (0) i.e. $(Real(Z_G(j\omega))Y_L(j\omega) < 0)$ and the lower part is the imaginary part $(Imaginary(Z_G(j\omega))Y_L(j\omega) = 0)$. Applying the criterion for different scenarios, the following results are obtained:

***Different current controller bandwidth*** $\alpha_{CC}$

Fig. 5.4 depicts the application of the Nyquist criterion for stability to the open loop system shown in Eqn. 4.3 in Section 4.1.3. The upper plot shows the real part of the open loop transfer function and the imaginary part is shown in the lower plot. It can be noticed that the lines of the imaginary part for the different $\alpha_{CC}$ cross the zero line at almost the same frequency, which means that for the three cases the system will have sub-synchronous oscillations at almost the same frequency (16 Hz) since all of the lines in the real part plot are below -1. However, looking at the real

part plot, it can be noticed that the lower the value of $\alpha_{CC}$, the more damping there is in the system, which means that higher $\alpha_{CC}$ values imply a system more prone to SSCI.

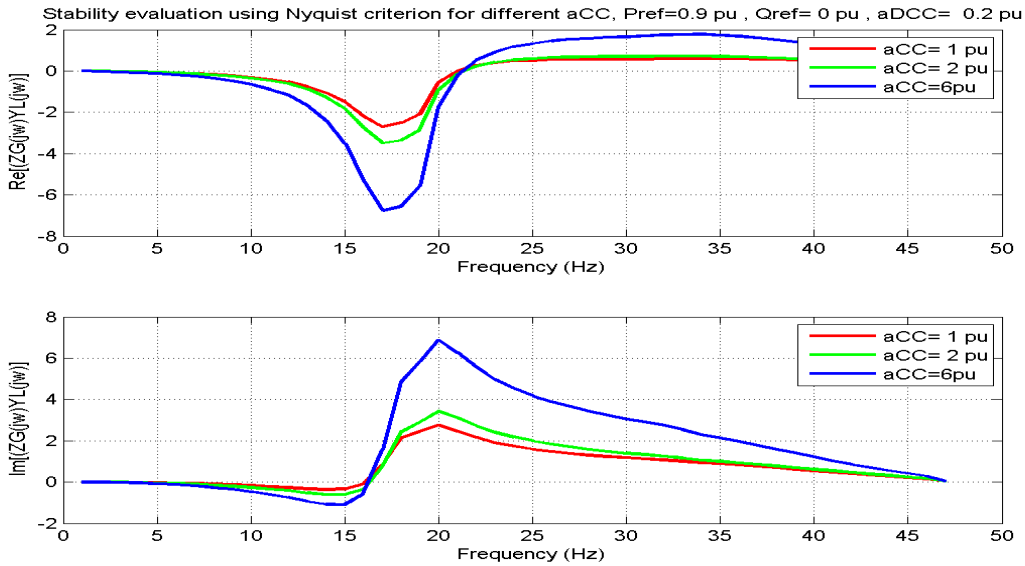


**Figure 5.4:** Evaluation of stability using Nyquist criterion for different current controller bandwidth $\alpha_{CC}$: upper plot: real part or open loop transfer function, lower part: imaginary part of open loop transfer function, $P = 0.9pu, Qref = 0pu$

***Different compensation levels:***

Fig. 5.5 illustrates the application of the criterion for different compensation levels, but for the same power and controller parameters. It is clear that in the case of no compensation, the system is stable since both real and imaginary parts are positive. The 8% compensation level shows a stable system as well since when the imaginary part crosses the 0, the real part is larger than -1. As for the compensation level of 25% and higher levels there is instability since for all these values, the real part is less than 1 when the imaginary part is 0. This implies less stable conditions and different frequencies of oscillations in case of SSCI.

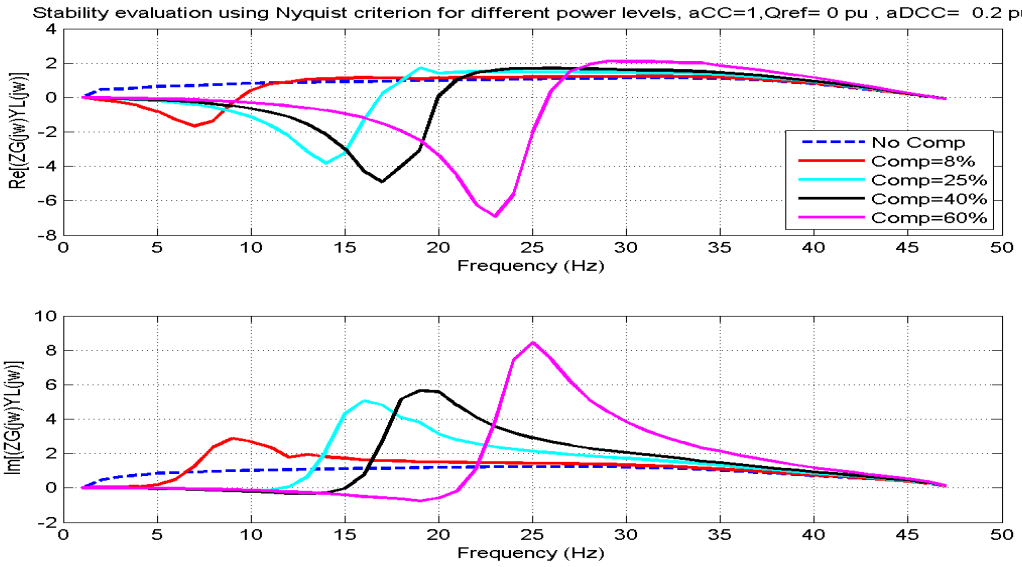


**Figure 5.5:** Evaluation of stability using Nyquist criterion for different compensation levels: upper plot: real part or open loop transfer function, lower part: imaginary part of open loop transfer function, $\alpha_{CC}, P = 0.9pu, Qref = 0pu$

## 5.2 Time-domain simulations

In this section, time domain simulations are be conducted in PSCAD/EMTDC. The SSCI event is created by opening the breaker $BRK\_SC$ in the circuit in Fig. 5.6.

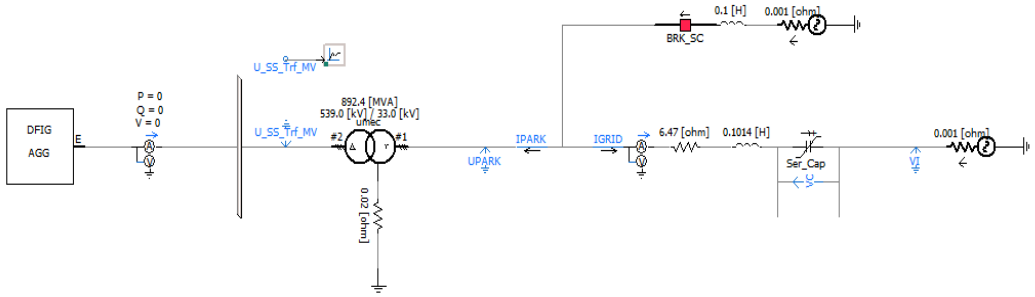


**Figure 5.6:** Screen print of the used IEEE FBM model

The event is created at 0.2 seconds. Opening the circuit breaker $BRK\_SC$ leaves the DFIG wind farm connected radially to the series-compensated line which resembles the first SSCI event in Zorillo. Different scenarios are simulated in the following.

### 5.2.1 Different power outputs

Cases are run for two different power outputs from the DFIG wind-farm. Both current controller bandwidth of DFIG and series compensation level are kept constant

($\alpha_{CC} = 1pu$ Compensation level % = 60%). Fig. 5.7 depicts the obtained results.

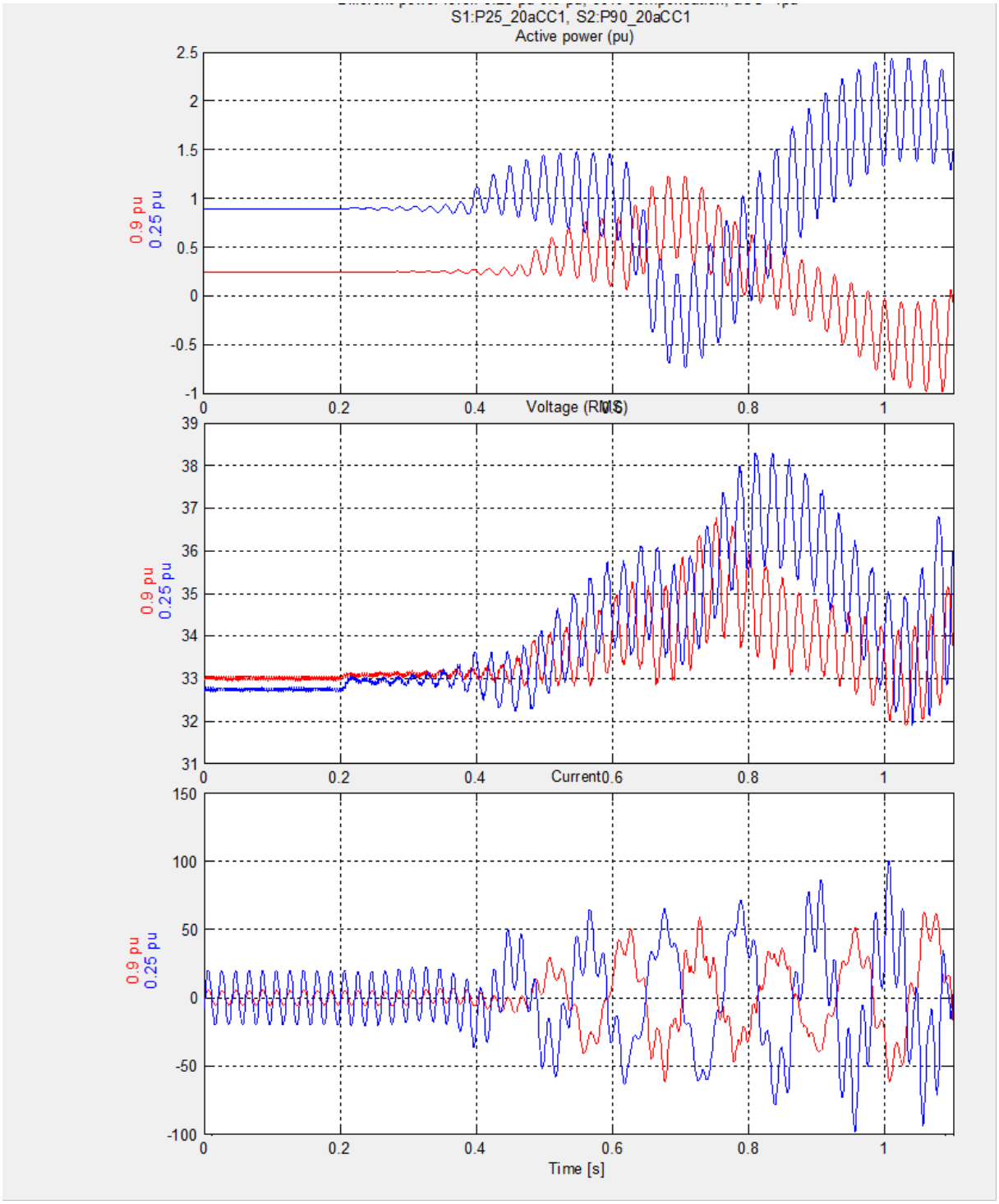


**Figure 5.7:** Different power reference: output power (top), terminal voltage and line current (bottom) Blue: $P_{ref} = 0.9$ pu, pu, Red: $P_{ref} = 0.25$ pu, $\alpha_{CC} = 2.0$ pu, Compensation=60%, $Q_{ref} = 0.0$ pu

It can be noticed that the different power references do not affect the frequency of the oscillations. However, the lower power output curve shows a faster build up of oscillations than the higher power output of 0.9 p.u. This shows that the operation

conditions of the DFIG wind farm connected to series-compensated line can affect the stability of the system: the higher the output power is, the more stable the system becomes.

### 5.2.2 Different current controller bandwidths ($\alpha_{CC}$)

For different values of DFIG current controller bandwidth ($\alpha_{CC}$), but fixed power output and compensation level, cases are run and the results are obtained for three values of $\alpha_{CC}$ (1,2, and 6 pu).

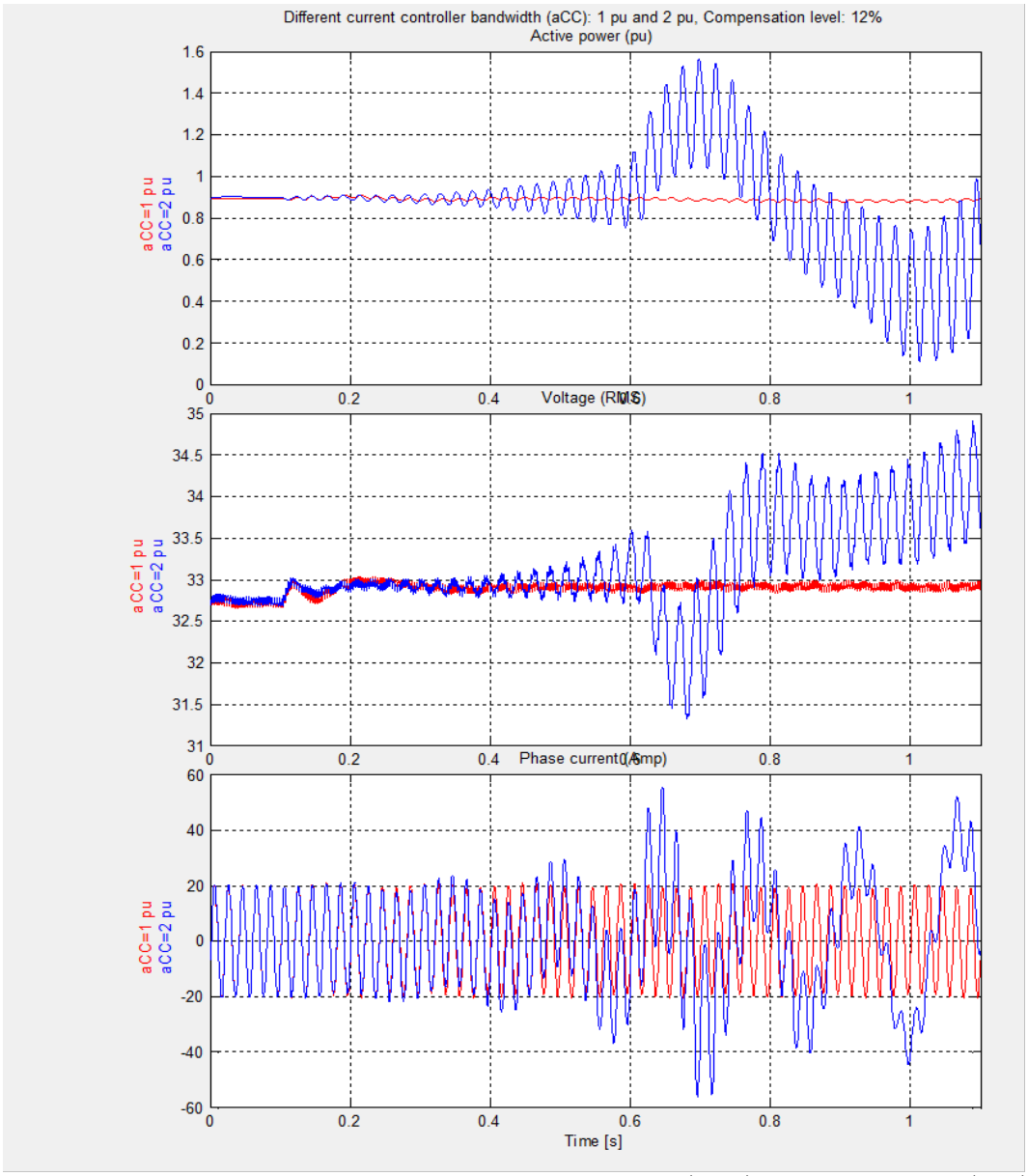


**Figure 5.8:** Different current controller bandwidth ($a_{CC}$): output power (top), terminal voltage and line current (bottom) Blue: $\alpha_{CC} = 2.0$ pu, Red: $\alpha_{CC} = 1.0$ pu, $P_{ref} = 0.9$ pu, $Q_{ref} = 0.0$ pu

Fig: 5.8 shows two lines for two different $\alpha_{CC}$: 1 pu and 2 pu for a certain compensation level (12%). It is clear that for a slower current controller ($\alpha_{CC} = 1$ pu), the system is stable and no growing oscillations show up, while for the same conditions, a DFIG with $\alpha_{CC} = 2$ pu, the system experiences sub-synchronous oscillations, which proves that the controller parameters are part of the SSCI problem.

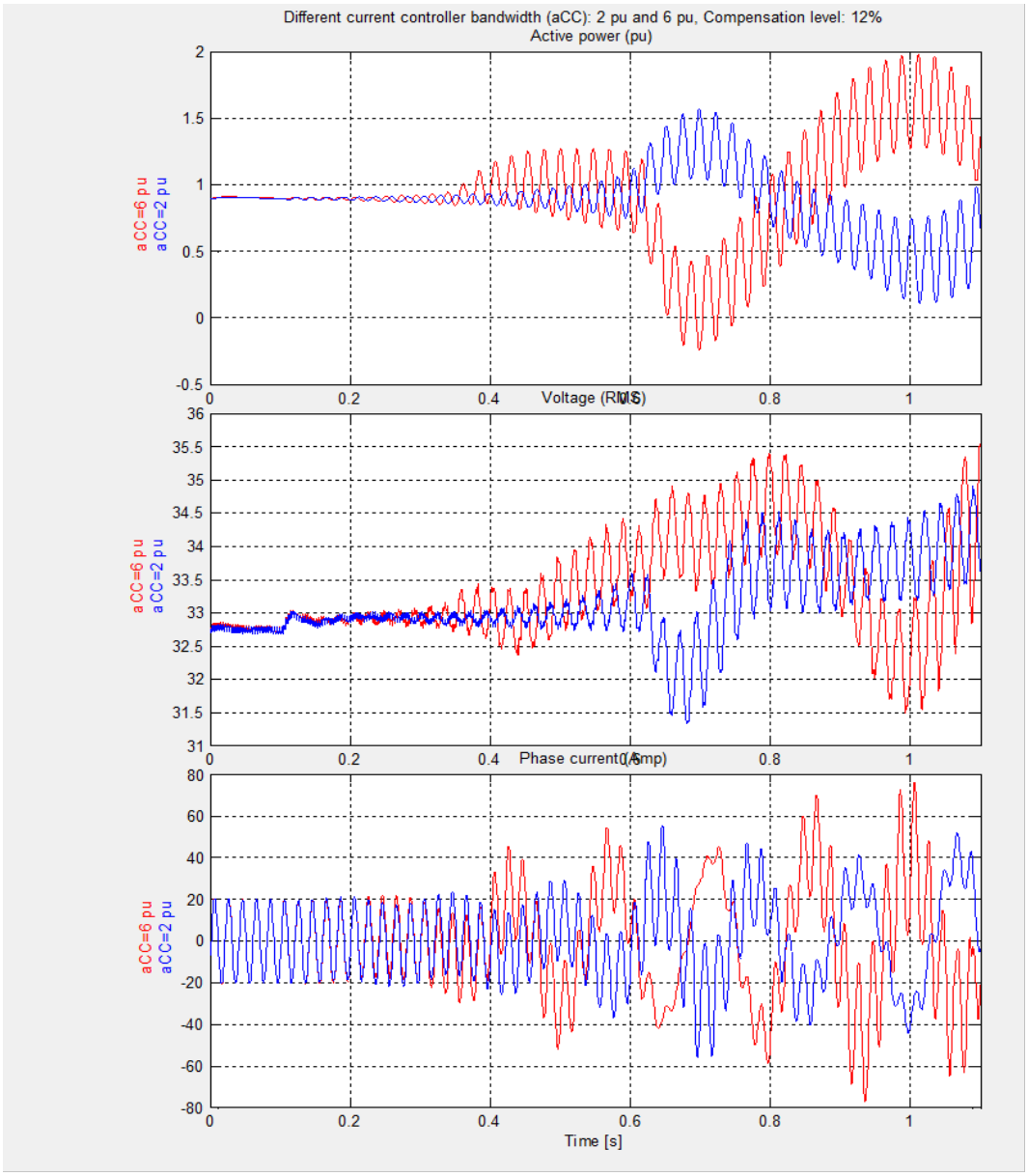


**Figure 5.9:** Different current controller bandwidth ($a_{CC}$): output power (top), terminal voltage and line current (bottom) Blue: $\alpha_{CC} = 2.0$ pu, Red: $\alpha_{CC} = 6.0$ pu, $P_{ref} = 0.9$ pu, $Q_{ref} = 0.0$ pu

Another scenario was to run two more cases: one with $\alpha_{CC} = 2$ pu and the other with $\alpha_{CC} = 6$ pu. It is noticed that the faster the current controller is the more severe the oscillations become in terms of speed of oscillation growth. Another aspect to be noticed is that for both cases, the frequency of oscillations is the same.

### 5.2.3 Different compensation levels

The series compensation level was changed for each case while keeping the output power and also the current controller bandwidth fixed.
Figures 5.10 and 5.11 show the effect of different compensation levels on the output power, line current and terminal voltage.

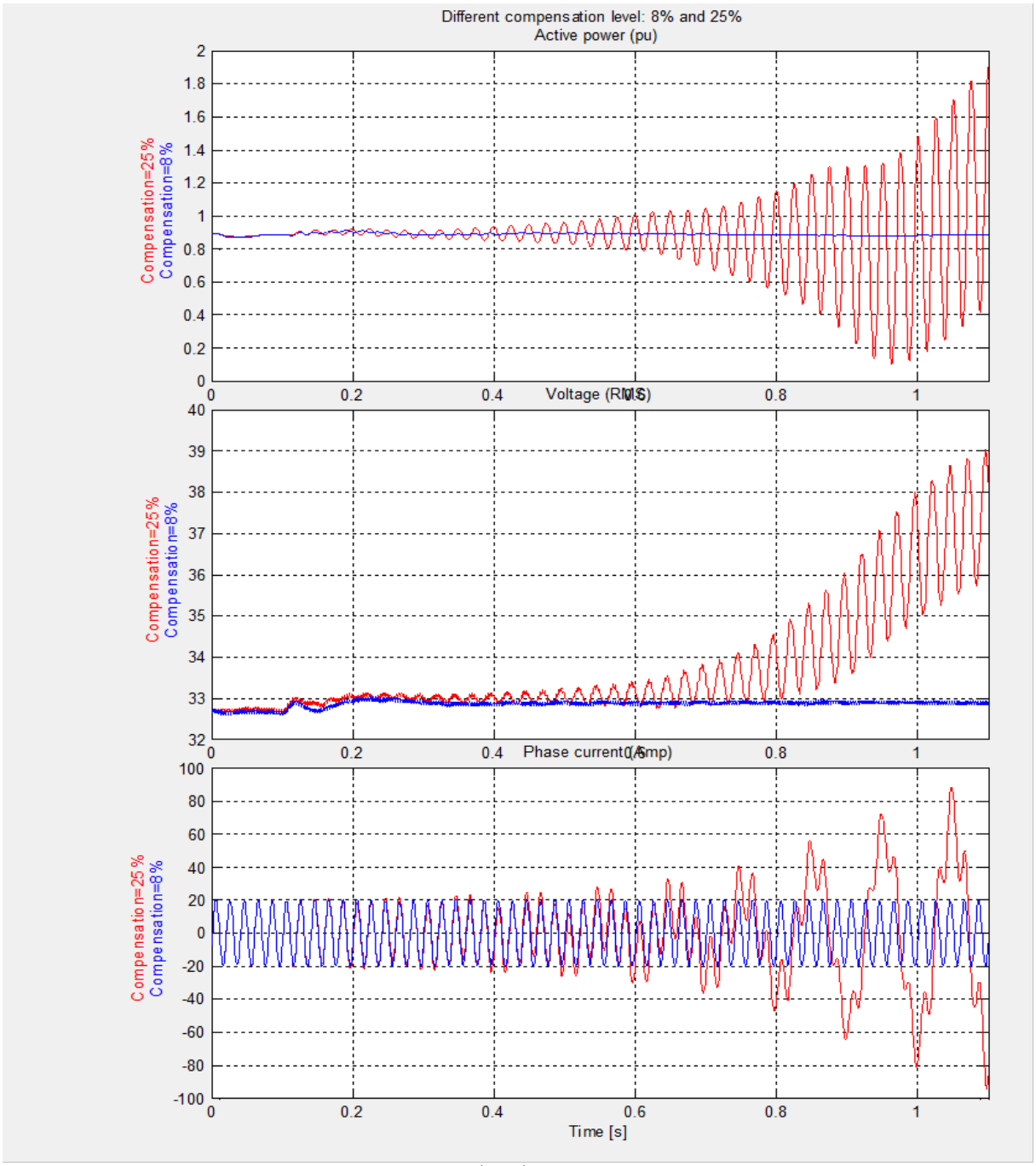


**Figure 5.10:** plots of output power (top), terminal voltage and line current (bottom) at the output of the aggregated wind farm after triggering oscillations at time 0.1 seconds. Blue: 8% compensation, Red: 25% compensation, $\alpha_{CC} = 1.0$ pu

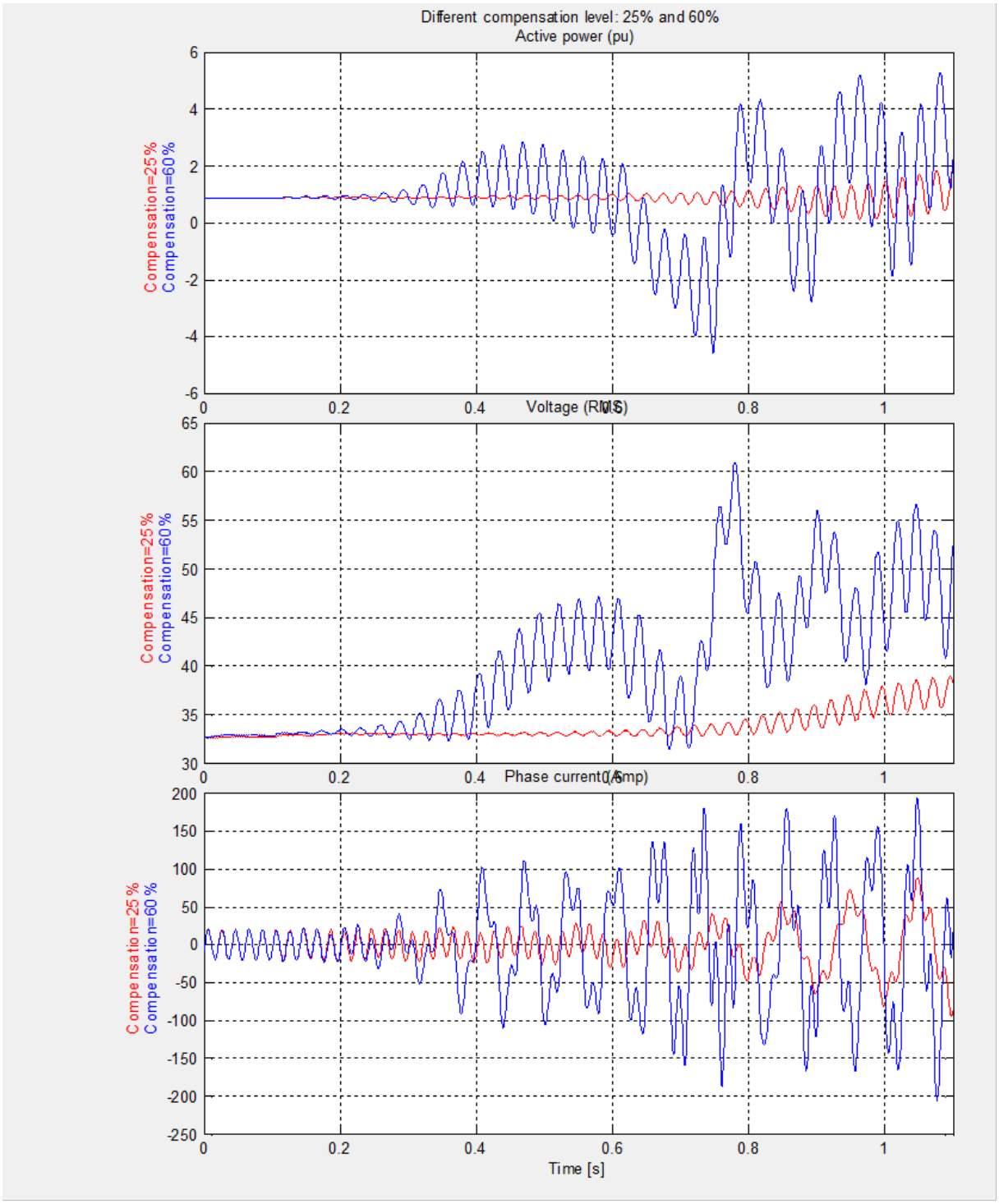


**Figure 5.11:** plots of output power (top), terminal voltage and line current (bottom) at the output of the aggregated wind farm after triggering oscillations at time 0.1 seconds. Blue: 25% compensation, Red: 60% compensation, $\alpha_{CC} = 1.0$ pu

The frequency of oscillations for each compensation level was recorded in the following table:

**Table 5.1:** Frequency of oscillation for different compensation levels

| Compensation level | Frequency |
|---|---|
| 8 % | 0 Hz |
| 25 % | 10.6 Hz |
| 40 % | 13.3 Hz |
| 60 % | 16.5 Hz |

## 5.3 Discussion

In the previous sections, two methods are applied to study SSCI in the IEEE FBM system. The first was a frequency domain method based on the net-positive damping criterion using Nyquist stability. The second is a time-domain method in which the system model in PSCAD/EMTDC was used, and then a contingency was created to render the DFIG radially connected to the series-compensated line. The following conclusions are made:

- The DFIG harmonic impedance scans show that the DFIG resistance is negative for the whole sub-synchronous range. Since in electrical systems the resistance is the damping parameter, then the presence of negative resistance implies growing oscillations instead of damping. This is the main issue regarding the DFIG wind-farm stability.

- In order for the electrical system not to experience SSCI, it should have net positive damping. This means that for the sub-synchronous range, if the system to which the DFIG is connected has positive resistance greater than the magnitude of the DFIG resistance in the sub-synchronous range, then the system will not suffer SSCI oscillations

- From time-domain simulations, it is seen that the factor that affects the oscillations' frequency and amplitude the most is the compensation level since it directly changes the impedance of the line and its resonance frequency. Also the $\alpha_{CC}$ affects the DFIG stability as it affects its impedance.

- DFIG wind farms exhibit varying negative resistance in the sub-synchronous range as the active power reference (wind speed in real life) varies. This implies the fact that the resonance conditions for DFIG-based wind-farm changes since the wind speed is not fixed. The plots show that low wind speeds represent more dangerous conditions for the occurrence of SSCI than larger speeds.However, the Nyquist plots show that the frequency of the oscillations for different power levels vary but very slightly.

- Another parameter that is interesting to notice is the effect of current controller bandwidth ($\alpha_{CC}$) change, which in our case affects only the dynamics of the RSC. It was shown in time-domain analysis that (for a certain compensation level) if the RSC current controller was slow enough, the system would be

stable, while for the same compensation level a faster current controller would laed to unstable sub-synchronous oscillations

- Effect of compensation level: The DFIG has negative resistance along the whole sub-synchronous frequency range, then the instability of the system depends on how much positive damping is offered by the electric network, which depends highly on the compensation level. Compensation level as well directly affects the resonant frequency as well. That's why according to Table 5.1, there are different oscillation frequencies for different compensation levels.

Comparing the time- and frequency-domain results, the following can be concluded:

- For the different $\alpha_{CC}$ cases, it was seen that the different $\alpha_{CC}$ do not affect the frequency of the oscillations which can be seen in Fig. 5.9 and Fig. 5.4. However, for faster current controllers, the system is more unstable and oscillations grow much faster.

- For the different compensation levels, both time and frequency domain simulations show that the higher the compensation level, the higher the frequency of oscillations, as seen in the two figures: Fig. 5.11 and Fig: 5.5

## 5.4 Damping of sub-synchronous oscillations with STATCOM

In this section, different scenarios will be presented to explore the behaviour of the DFIG in case of radial connection to series-compensated transmission line and the presence of 150 MVAR STATCOM at the wind farm bus. The scenarios will include the operation of STATCOM on voltage control and the inclusion of SSDC (Sub-Synchronous Damping Controller). Also, the change of compensation levels, DFIG current controller parameters and power reference. Moreover the system's behaviour to re-closing of the breaker will be studied. In the following, SSDC refers to Sub-Synchronous Damping Controller (as used in many papers), which refers to the controller used to modulate the STATCOM voltage reference in order to damp the sub-synchronous oscillations.

### 5.4.1 STATCOM with voltage control only

First, the effect of the STATCOM at the wind farm bus with only voltage control is studied.

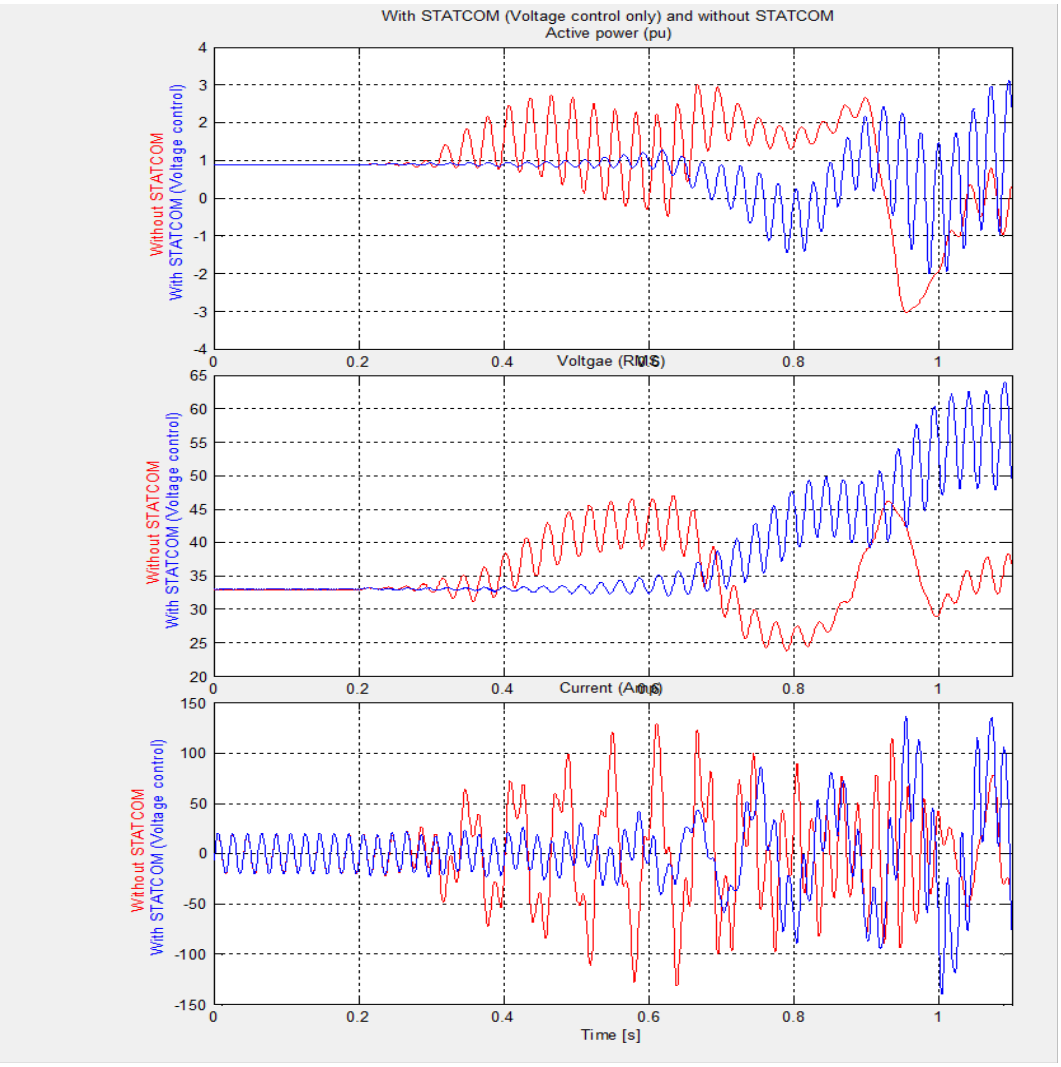


**Figure 5.12:** Plots of: output power (top), terminal voltage (middle) and line current (bottom) of the DFIG after triggering oscillations at time 0.2 seconds. Blue: With STATCOM ($P_{ref}$ = 0.9 pu, $Q_{ref}$ = 0.0), Red: No STATCOM

In Fig. 5.4.1 it can be noticed that even without adding any sub-synchronous damping loop. This can be attributed to the filters connected to the STATCOM. Since the STATCOM is connected at the DFIG plant bus, then they can affect the impedance seen by the network at the DFIG bus.

### 5.4.2 STATCOM with voltage control only for different $\alpha_{CC}$ values

To check the effect of the DFIG control parameters on the STATCOM ability to damp the oscillations, the scenario depicted in Fig: 5.13 was studied

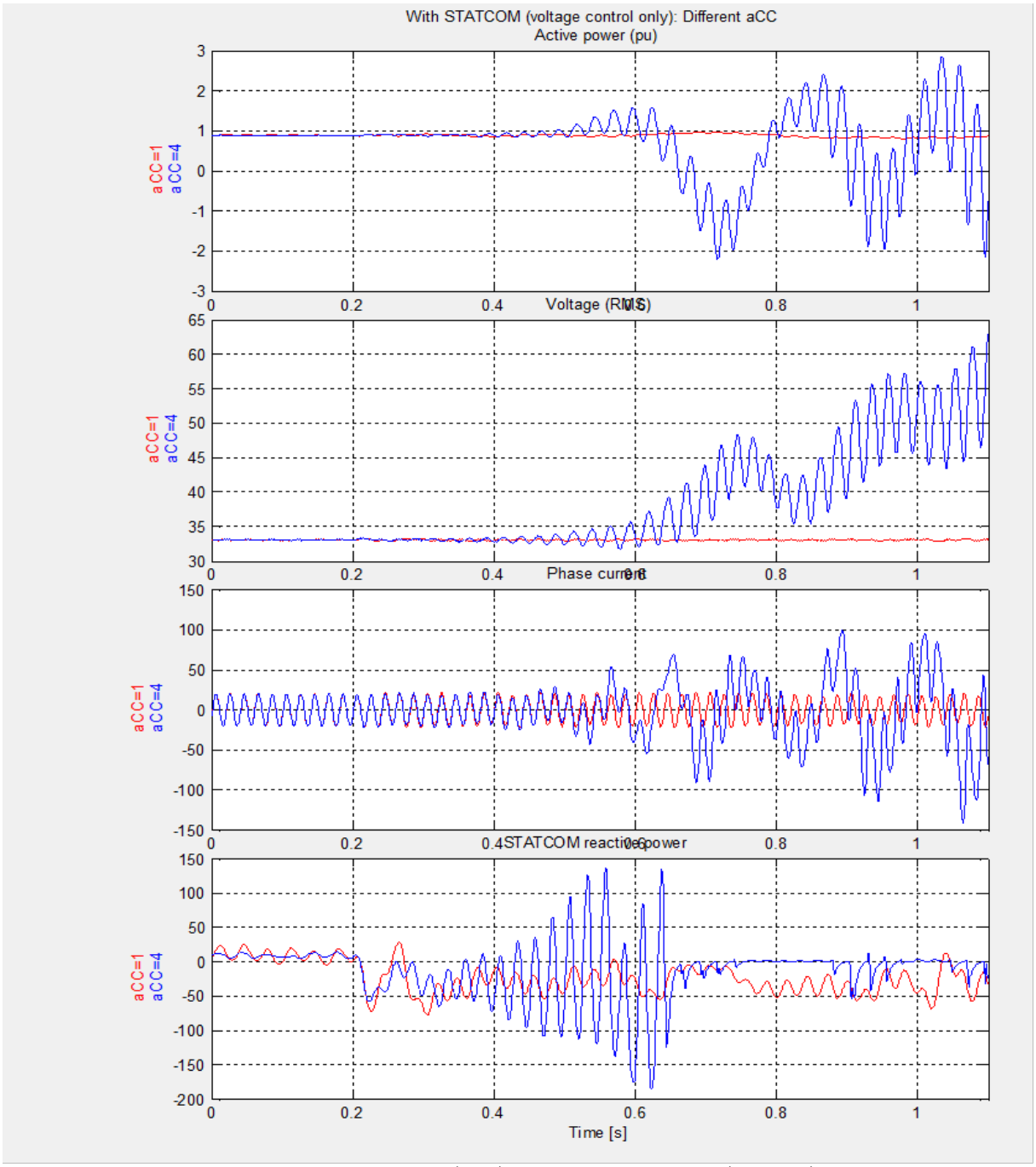


**Figure 5.13:** Plots of: output power (top), terminal voltage (second), line current (third), STATCOM reactive power (bottom) triggering oscillations at time 0.2 seconds. Blue: $\alpha_{CC} = 4$ , Red: $\alpha_{CC} = 1$, $P_{ref} = 0.9$ pu, $Q_{ref} = 0.0$ pu

It can be seen that for slow DFIG controller ($\alpha_{CC} = 1$), the presence of the STATCOM (and its filters) added damping to the system (for compensation level=60% and output power=0.9pu) without even the need for the SSDC (the red line in the figure). While for faster current controller, the STATCOM (plus its filters) could not do the task.

### 5.4.3 STATCOM with SSDC

The controller discussed in Chapter 4 was added to the STATCOM connected to the wind farm bus and applied to damp the SSO.
As depicted, the controller was started at $t \approx 0.3s$. Note that in this way, the STATCOM was able to damp the oscillations both in voltage and current output of the DFIG after triggering the event at $t \approx 0.2s$. The bottom figure shows the reactive power injected by the STATCOM to damp the oscillations by controlling the voltage at the connection point.

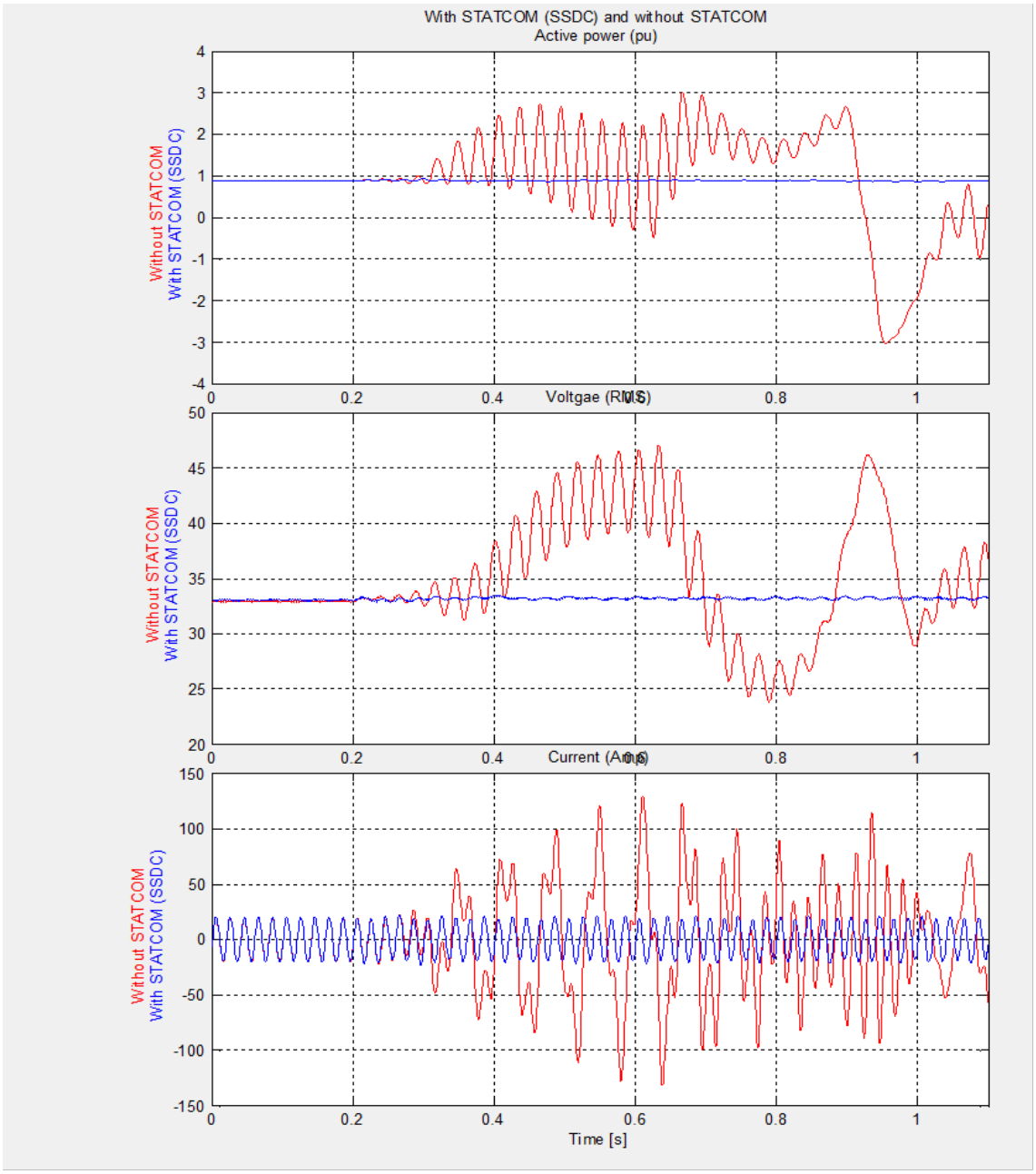


**Figure 5.14:** Plots of: output power (top), terminal voltage (second), line current (third), STATCOM reactive power (bottom) triggering oscillations at time 0.2 seconds. Blue: With STATCOM (plus SSDC), Red: Without STATCOM, $P_{ref} = 0.9$ pu, $Q_{ref} = 0.0$ pu

It is also interesting to compare the effect of the STATCOM with and without the SSDC in Fig: 5.15 below.
The figure shows the effects of the STATCOM SSDC which is clear in damping the oscillations in both current and voltage.
An interesting aspect to be noticed is that the controller not only adds the proper amplitude of reactive power, but also the proper phase shift, which is a very important feature to follow the fast changing oscillations.

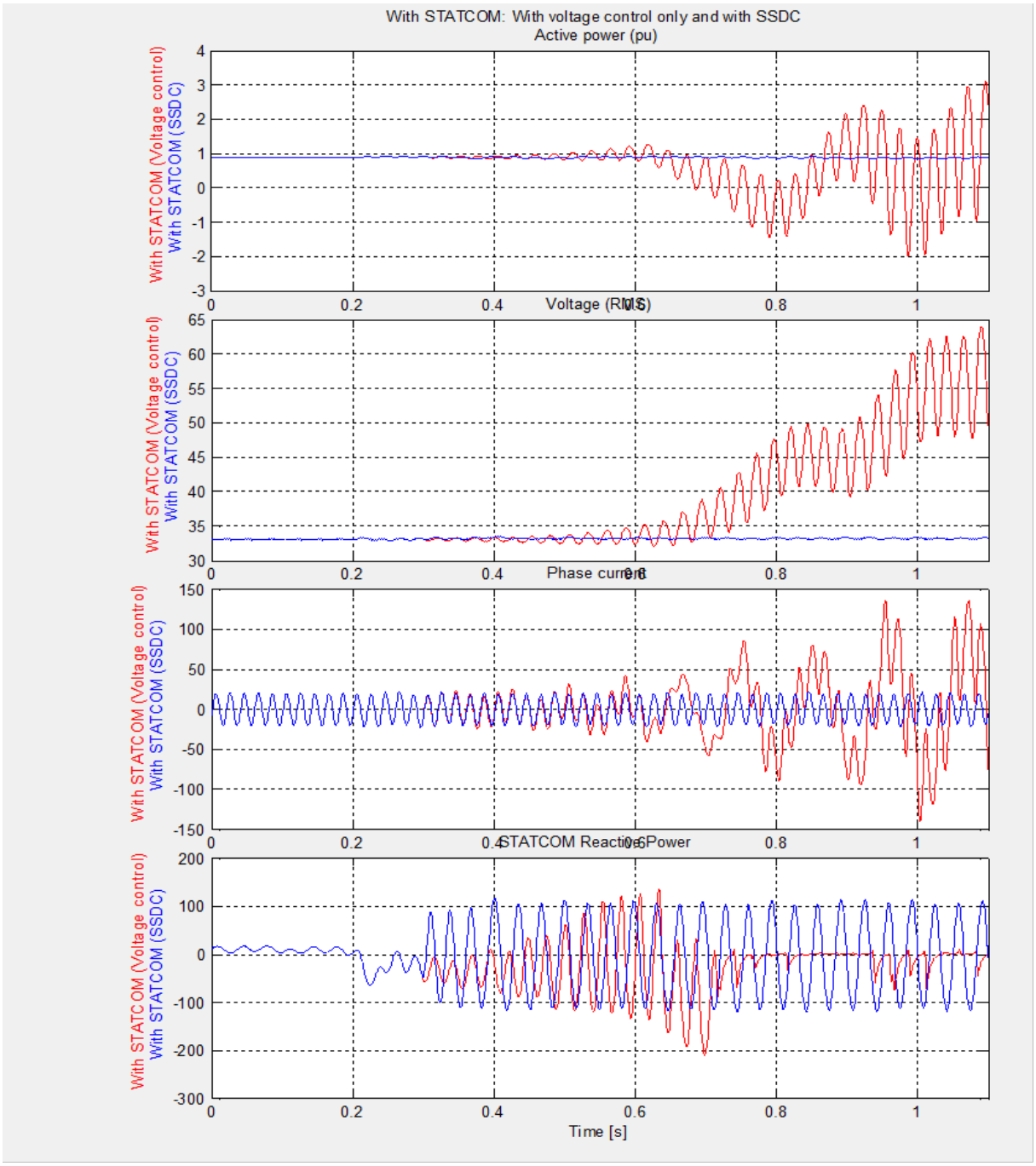


**Figure 5.15:** Plots of: output power (top), terminal voltage (second), line current (third), STATCOM reactive power (bottom) triggering oscillations at time 0.2 seconds. Blue: With STATCOM (plus SSDC), Red: With STATCOM (voltage control only)

### 5.4.4 Re-closing the breaker

It is interesting to see the effect of the STATCOM on the stability of the system after re-closing the breaker (after the oscillations had started to grow). In this case, it is only the impact of the STATCOM voltage controller to be investigated (SSDC is disabled).

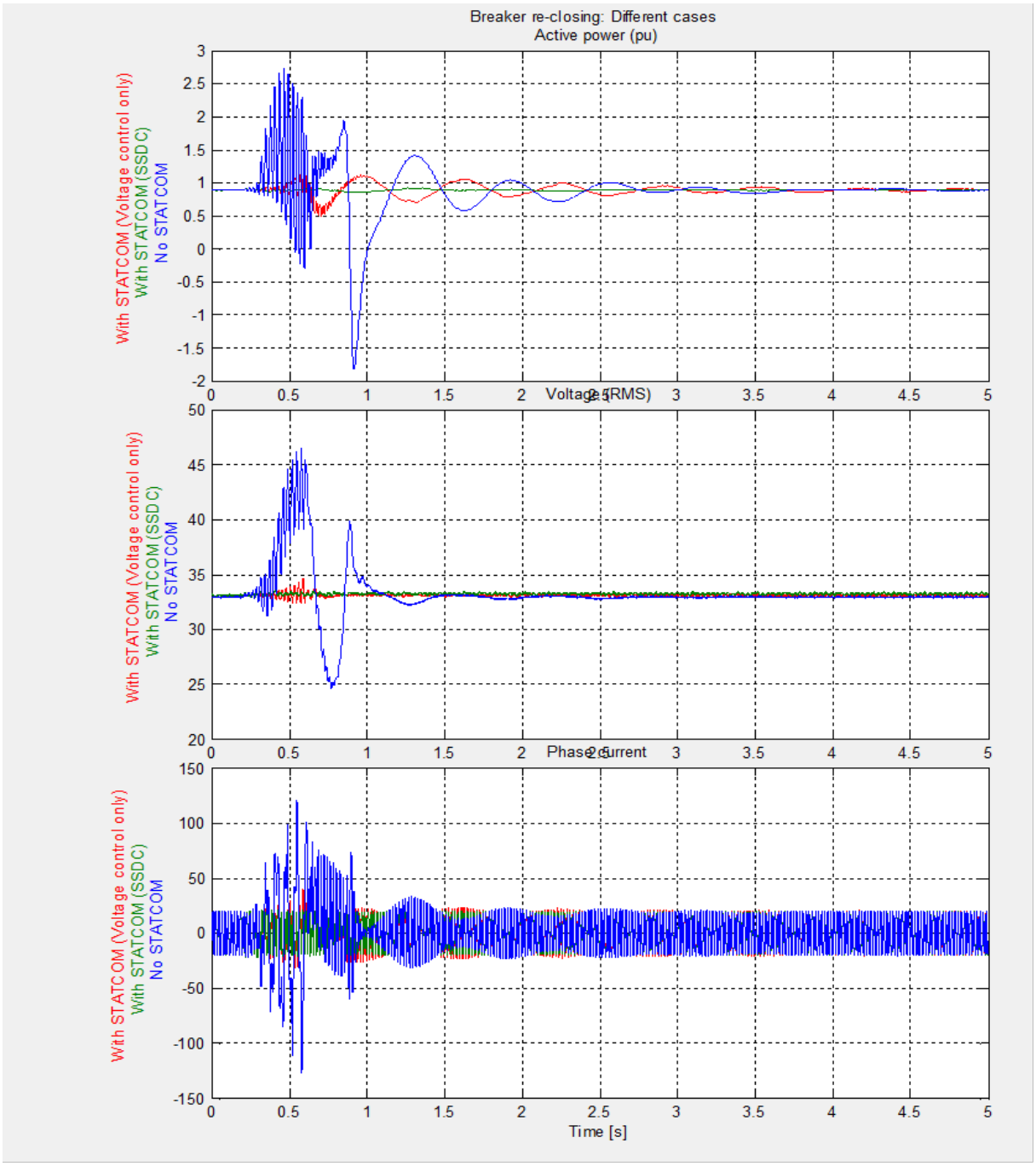


**Figure 5.16:** Plots of: output power (top), terminal voltage (second), line current (third), STATCOM reactive power (bottom) triggering oscillations at time 0.2 seconds. Blue: Without STATCOM , Red: With STATCOM (voltage control only),Green: STATCOM (with SSDC)

In Fig. 5.16, it is clear that the STATCOM improves the system's stability by adding damping to the oscillations. The event was established at 0.2 seconds and the breaker was re-closed at 0.6 seconds. The effect is very clear in the magnitude of the overshoot that the system experiences in both cases. It is obvious that STATCOM adds very considerable damping to the oscillations even without the SSDC loop. However, as previously explained, this damping comes from the STATCOM filters which change the impedance seen by the network from the DFIG bus. Adding the activation of the SSDC loop gives more stable performance, which can be noticed in the green line in the same figure.

## 5.5 Conclusions

In this chapter, the SSCI of DFIG-based wind farm connected to a series-compensated transmission line has been investigated. The analysis is conducted in both time-domain and frequency-domain to gain more insight of the reasons behind the sub-synchronous phenomenon. The following conclusions can be listed:

1. For the study, the IEEE FBM for SSR computer studies was used and modified for the specific analysis. This was done by replacing the synchronous machine with an aggregated DFIG wind farm. All of the simulations are in PSCAD/EMTDC.

2. Frequency domain studies showed that the DFIG exhibits negative resistance along the whole sub-synchronous range, which is the main reason that causes the instability. This means that the presence of DFIG actually adds negative damping to the network at this frequency range.

3. Different parameters affect the oscillations levels, speed of growing and frequency. These parameters are: level of series capacitive compensation, DFIG control parameters and power level.

4. The faster the DFIG RSC current controller is (larger $\alpha_{CC}$), the more likely it is that the system will suffer SSCI. This is shown by noticing how the change of $\alpha_{CC}$ affects the impedance of the DFIG. The faster the current controller is, the more negative the DFIG resistance is which makes the DFIG system more prone to susb-synchronous stability. This however does not affect the frequency of the oscillations.

5. The higher the compensation level, the more likely it is that oscillations will occur. Also, this leads to an increase of the frequency of oscillations.

6. Finally, the STATCOM was used to successfully damp the SSO and different cases are presented.

# 6

# Conclusions and future work

## 6.1 Conclusions

In this thesis the sub-synchronous controller interaction (SSCI) of a DFIG wind farm connected to a series compensated transmission line has been studied. The IEEE FBM for SSR studies is used; the synchronous generator in the original model was replaced by a DFIG wind farm. For the simulations, PSCAD/EMTDC is used for the whole study.

The first part of the thesis is dedicated to the analysis, in order to provide understanding of the SSCI phenomenon. This is done both in frequency-domain and time-domain. Frequency-domain analysis is conducted in two steps:

1. By doing impedance-frequency scan of the DFIG wind farm. It is found that the DFIG wind farm exhibits negative resistance (real part of the impedance) in the sub-synchronous frequency range. This proves that the DFIG contributes to the problem of instability at this frequency range since it adds negative damping, which could lead to growing oscillations. It is also found that different parameters affect this impedance, in particular the RSC current controller bandwidth. The faster this controller is, the more negative the resistance becomes. Also, the DFIG reference power is found to have an effect on the impedance as well: the lower the power reference is, the more negative the resistance becomes.

2. By applying the net-positive damping criterion on the closed loop system of the DFIG-network. The Nyquist criterion is used for this and it is shown that the DFIG RSC controller bandwidth affects SSCI as well as the series-compensation level, which is proven to affect the frequency of oscillations very significantly.

As for time domain analysis, it is simply done by running the simulations and applying the condition that creates the oscillations. Different cases are studied for different RSC current controller bandwidths, different compensation levels and different

power reference levels. The same conclusions are made as in the frequency-domain analysis.

The second part of thesis is to use the STATCOM in damping the oscillations. A novel controller is implemented, which first detects the presence of sub-synchronous oscillations in the voltage or current signal by extracting its envelope waveform. Then, after the current exceeds a certain threshold, the frequency of the envelope is estimated and after that this estimation is used to extract the power component of that frequency. This signal is further multiplied by an empirical constant (found by trial and error) and then used to modulate the STATCOM voltage reference.

Satisfactory results are obtained as the oscillations of power and voltage are damped for different scenarios.

## 6.2 Future work

Different aspects could be further studied such as making use of the impedance-frequency scan of the DFIG in damping the oscillations. This can be done by obtaining an impedance scan of the connected STATCOM and its control so that the total resistance of the DFIG+STATCOM combination becomes positive for the sub-synchronous frequency range.

Another interesting thing to be investigated is to systematically select the damping signal. Different tests can be done using other signals such as frequency or voltage. The gain of the power signal that modulates the voltage reference can also be selected in a more systematic way such as optimal tuning of a PI controller to obtain more robust results.

Another area that could be studied is the behaviour of the DFIG for frequencies above synchronous frequencies (maybe a up until a few multiples of the base frequencies) as it has been shown in some publications that a grid-connected VSC has a negative input admittance for frequencies higher than the fundamental [15]. The case studied here would be the interaction of the DFIG with nearby LC filters tuned to some harmonic frequencies. An event can be created that renders the DFIG closely connected to the LC filter.

# Bibliography


[1] J. R. Buck A. V. Oppenheim R. W. Schafer. *Discrete-time signal processing.* Prentice-Hall: Upper Saddle River, 2001.

[2] J.A. Solsona A.E. Leon. "Sub-Synchronous Interaction Damping Control for DFIG Wind Turbines". In: *IEEE TRANSACTIONS ON POWER SYSTEMS* (2015).

[3] E. H. Camm et al. "Reactive power compensation for wind power plants". In: *2009 IEEE Power Energy Society General Meeting* (2009), pp. 1–7. DOI: 10.1109/PES.2009.5275328.

[4] L. Ängquist. "Synchronous Voltage Reversal Control of Thyristor Controlled Series Capacitor". PhD thesis. 2002.

[5] S.Saylors B.Badrzadeh. "Susceptibility of wind turbines to sub-synchronous control and torsional interaction". In: *Transmission and Distribution Conference and Exposition* (2012). DOI: 10.1109/TDC.2012.6281605.

[6] M. E. H. Benbouzid. "A Review of Induction Motors Signature Analysis as a Medium for Faults Detection". In: *EEE Trans. Industrial Electronics* (2000), pp. 984–993.

[7] M. Beza. "Power System Stability Enhancement Using Shunt-connected Power Electronic Devices with Active Power Injection Capability". PhD thesis. 2015.

[8] M. Bongiorno. "On Control of Grid-connected Voltage Source Converters: Mitigation of Voltage Dips and Subsynchronous Resonances". PhD thesis. 2007.

[9] S. Chernet. "Subsynchronous Resonance in Doubly-Fed Induction Generator Based Wind Farms". PhD thesis. 2016.

[10] Global Wind Energy Council. *GLOBAL WIND STATISTICS 2015.* URL: http://www.gwec.net/wp-content/uploads/vip/GWEC-PRstats-2015_LR_corrected.pdf.

[11] *EMTDC User's Guide.* Manitoba HVDC Research Centre Inc, 2005.

[12] C. Heyman H. Xie M.M. Oliveira. "Mitigation of Sub-Synchronous Resonance in a DFIG-Based Wind power plant connected to series-compensated lines using STATCOM". In: *IET Renewable Power Generation* (2014).

[13] M.M. Oliveira H. Xie. "Mitigation of SSR in Presence of Wind Power and Series Compensation by SVC". In: *International Conference on Power System Technology (POWERCON 2014)* (2014).

[14] M. C. Hall and D. A. Hodges. "Experience with 500-kV Subsynchronous Resonance and Resulting Turbine Generator Shaft Damage at Mohave Generating

Station". In: *IEEE PES Special Publication, Analysis and Control of Subsynchronous Resonance* (1976).

[15] L. Harnefors. "Passivity-Based Stability Assessment of Grid-Connected VSCs—An Overview". In: *IEEE JOURNAL OF EMERGING AND SELECTED TOPICS IN POWER ELECTRONICS* (2016).

[16] L. Harnefors. "Proof and Application of the Positive-Net-Damping Stability Criterion". In: *IEEE TRANSACTIONS ON POWER SYSTEMS* (2011), pp. 481–482. DOI: 10.1109/TPWRS.2010.2052965.

[17] L. Hingorani N. ; Gyugyi. *Understading FACTS*. Wiley-IEEE Press, 2000. ISBN: 9780470546802.

[18] G.D. Irwin; A.K Jindal; A.L. Isaacs. "Sub-synchronous control interactions between type 3 wind turbines and series compensated AC transmission systems". In: *2011 IEEE Power and Energy Society General Meeting* (2015), pp. 1–6. DOI: 10.1109/PES.2011.6039426.

[19] P Kundur. *Power System Stability and Control*. Mcgraw Hill, 1994. ISBN: 007035958X.

[20] E. V. Larsen. "Wind generators and series-compensated AC transmission lines". In: *Transmission and Distribution Conference and Exposition (TD), 2012 IEEE PES* (2012), pp. 1–4. DOI: 10.1109/TDC.2012.6281548.

[21] JR LAWRENCE C. GROSS. "A Generic DFIG Model for Voltage Dip Ride-Through Analysis". In: *IEEE TRANSACTIONS ON ENERGY CONVERSION* 28.1 (2013), pp. 76–85. DOI: 10.1109/TEC.2012.2222885.

[22] E. Agneholm M. Bongiorno and A. Petersson. "The impact of Wind Farms on Subsynchronous Resonance in Power Systems". In: *Elforsk rapport 11:29* (2009).

[23] MatLab. *Envelope Detection*. URL: http://se.mathworks.com/help/dsp/examples/envelope-detection.html.

[24] H. T. Ma; P. B. Brogan; K. H. Jensen; R. J. Nelson. "Sub-Synchronous Control Interaction studies between full-converter wind turbines and series-compensated AC transmission lines". In: *IEEE Power and Energy Society General Meeting* (2012), pp. 1–5. DOI: 10.1109/PESGM.2012.6345523.

[25] Paul M. Anderson; B. L. Agrawal; J. E. Van Ness. *Subsynchronous resonance in power systems*. Wiley-IEEE Press, 1990. ISBN: 9780470546505.

[26] A. PETERSSON. "Analysis, Modeling and Control of Doubly-Fed Induction Generators for Wind Turbines". PhD thesis. 2005.

[27] S. Auddy R. K. Varma. "Mitigation of subsynchronous resonance by SVC using PMU-acquired remote generator speed". In: *IEEE Power India Conference* (2006). DOI: 10.1109/POWERI.2006.1632626.

[28] Y. Semsedini R.K. Varma S. Auddy. "Mitigation of Subsynchronous Resonance in a Series-Compensated Wind Farm Using FACTS Controllers". In: *IEEE TRANSACTIONS ON POWER DELIVERY* 23.3 (2008), pp. 1645–1654. DOI: 10.1109/TPWRD.2008.917699.

[29] M. Bongiorno S. Chernet. "Input Impedance Based Nyquist Stability Criterion for Subsynchronous Resonance Analysis in DFIG Based Wind Farms". In: *2015 IEEE Energy Conversion Congress and Exposition (ECCE)* (2015). DOI: 10.1109/ECCE.2015.7310541.

[30] Y. Semsedini S. K. Varma S. Auddy. “Mitigation of Subsynchronous Resonance in a Series-Compensated Wind Farm Using FACTS Controllers”. In: *IEEE TRANSACTIONS ON POWER DELIVERY* 23.3 (2008), pp. 1645–1654. DOI: DOI:10.1109/TPWRD.2008.917699.

[31] IEEE Subsynchronous Resonance Working Group of the System Dynamic Performance Subcommittee. “READER’S GUIDE TO SUBSYNCHRONOUS RESONANCE”. In: *IEEE Transactions on Power Systems* 7.1 (1992), pp. 150–157. DOI: 10.1109/59.141698.

[32] Subsynchronous Resonance Working Group of the System Dynamic Performance Subcommittee. “READER’S GUIDE TO SUBSYNCHRONOUS RESONANCE”. In: *IEEE Transactions on Power Systems* 7.1 (1992), pp. 150–157. DOI: 10.1109/59.141698.

[33] A. Ukil. “Time-Domain Estimation of Sub-harmonic Sinusoidal Disturbance in Sinusoidal Signal with Applications in Induction Motor Diagnostics”. In: *Electrical Machines (ICEM), 2012 XXth International Conference on* (2012), pp. 1899–1905. DOI: 10.1109/ICElMach.2012.6350141.